AFOSR-TR- 82-0673

(14)

DEFLAGRATION-TO-DETONATION IN HMX-BASED PROPELLANTS

Final Report
Covering the Period January 1, 1977 to November 1, 1981

March 1982

By: M. Cowperthwaite and W. J. Murri

Prepared for:

AIR FORCE OFFICE OF SCIENTIFIC RESEARCH/NA
Bolling Air Force Base, D.C. 20322

Attention: Dr. L. H. Caveny

Contract No. F49620-77-C-0039

SRI Project PYU 6069

SRI International
333 Ravenswood Avenue
Menlo Park, California 94025
(415) 326-6200
TWX: 910-373-2046
Telex: 334 486

UNCLASSIFIED

SECURITY CLASSIFICATION OF THIS PAGE *(When Data Entered)*

REPORT DOCUMENTATION PAGE	READ INSTRUCTIONS BEFORE COMPLETING FORM
1. REPORT NUMBER: AFOSR-TR- 82-0673	2. GOVT ACCESSION NO.: AD-A118616
	3. RECIPIENT'S CATALOG NUMBER:
4. TITLE *(and Subtitle)*: DEFLAGRATION-TO-DETONATION IN HMX-BASED PROPELLANTS	5. TYPE OF REPORT & PERIOD COVERED: Final Report - January 1, 1977 to November 1, 1981
	6. PERFORMING ORG. REPORT NUMBER: PYU-6069
7. AUTHOR(s): M. Cowperthwaite and W. J. Murri	8. CONTRACT OR GRANT NUMBER(s): F49620-77-C-0039
9. PERFORMING ORGANIZATION NAME AND ADDRESS: SRI International, 333 Ravenswood Avenue, Menlo Park, CA 94025	10. PROGRAM ELEMENT, PROJECT, TASK AREA & WORK UNIT NUMBERS: 61102F 2308/A1
11. CONTROLLING OFFICE NAME AND ADDRESS: Air Force Office of Scientific Research, Bolling Air Force Base, D.C. 20322	12. REPORT DATE: March 1982
	13. NUMBER OF PAGES: 80
14. MONITORING AGENCY NAME & ADDRESS *(if different from Controlling Office)*	15. SECURITY CLASS *(of this report)*: Unclassified
	15a. DECLASSIFICATION/DOWNGRADING SCHEDULE

16. DISTRIBUTION STATEMENT *(of this Report)*

Approved for public release; distribution unlimited.

17. DISTRIBUTION STATEMENT *(of the abstract entered in Block 20, if different from Report)*

18. SUPPLEMENTARY NOTES

19. KEY WORDS *(Continue on reverse side if necessary and identify by block number)*

HMX-based propellants
Reactive discontinuities
Hugoniot curves
Detonation
Deflagration
Accelerating flames
Shock formation
Lagrange stress gages
Stress histories
Lagrange analysis

20. ABSTRACT *(Continue on reverse side if necessary and identify by block number)*

The objective of the research was to develop the capability of assessing the deflagration-to-detonation transistion (DDT) hazard in HMX-based propellants. Theoretical and experimental studies were undertaken to elucidate mechanisms of DDT, to establish conditions for its occurrence, and to formulate a satisfactory model for its quantitative description.

cont.

DD FORM 1 JAN 73 1473 EDITION OF 1 NOV 65 IS OBSOLETE

UNCLASSIFIED

SECURITY CLASSIFICATION OF THIS PAGE *(When Data Entered)*

cont.

The theoretical studies were concerned with the thermo-hydrodynamic treatment of DDT. Equations governing flames treated as reactive discontinuities were derived, and conditions were established for shock formation in front of an accelerating flame. Model solutions to the one-dimensional equations governing an accelerating flame in a closed table were constructed and examined to gain an insight into DDT. These solutions demonstrate that DDT strongly depends on the burning rate and will probably not occur unless the burning rate parameter exceeds a value of approximately 1.0×10^{-2} mm/μs kbar.

In the experimental study, an assembly was designed to allow incorporation of stress gages into propellant charges during the casting process, thereby eliminating the expensive machining and grooving operations conventionally used in constructing targets for Lagrange gage experiments. The gage configuration designed for the DDT experiments was validated in gas gun experiments.

DDT experiments were performed in steel and Lexan confinement with propellant supplied by Edwards Air Force Base. DDT was not observed in cast propellant in either steel or Lexan confinement, but probably did occur in one of the experiments performed with powdered propellant in Lexan confinement. However, internal pressure histories were recorded for the first time in a DDT experiment in the compressed propellant confined by steel. The gages recorded time periods of 300-500 μs, and peak pressure in the 2.5 to 4 kbar region. The limited pressure buildup is attributed to the small percentage of HMX in the propellant. A shock was not formed ahead of the flame because the second derivative of the Lagrange pressure-specific volume compression curve is negative in this pressure region. The DDT experiments performed in Lexan tubes with propellant containing 50% HMX were unsuccessful as Lagrange gage experiments because the flow was not one dimensional. No comparison of theoretical and experimental results was possible because DDT was not observed in a one-dimensional experiment. DDT experiments with propellant containing 50% HMX confined in steel tubes are recommended for any such Lagrange gage experiments that may be undertaken in the future.

CONTENTS

ILLUSTRATIONS

TABLES

I INTRODUCTION AND OBJECTIVES

Research on the deflagration-to-detonation transition (DDT) is important to the Air Force because many of the energetic propellants required for present and future long-range delivery systems are readily detonable, can be used as good explosives, and as such are capable of undergoing DDT. Rockets motors burning HMX-based propellant have, for example, been destroyed by DDT on several occasions. Possible steps leading to detonation in the rocket motor are fracture of propellant ahead of the flame and the subsequent formation of shock waves produced by the increased burning rate of fractured propellant. However, in this important case, the mechanism of DDT and the conditions for its initiation are not adequately understood.

The long-range objective of the present research program is to develop a computational capability for assessing the DDT hazard in explosively filled propellants. The program is based on the concept that the physical and chemical processes involved in DDT must be identified, understood, and incorporated into a realistic model of DDT before the objective can be achieved. Theoretical and experimental work was undertaken to model and establish conditions for the onset and occurrence of DDT in HMX-based propellants. The goal of the theoretical work is to formulate a realistic model for the flow produced by an unsteady flame propagating in propellant contained in a closed tube. The goal of the experimental work is to perform Lagrange stress gage experiments to quantify states attained ahead of the flame front in burning HMX propellant, to establish conditions for the onset of DDT, and to provide data for the modeling effort.

II THEORETICAL WORK

Our theoretical study was concerned with DDT in a burning propellant contained in a closed tube. A phenomenological approach was taken to:

- Develop a physical understanding of the thermo-hydrodynamics of the flame, its propagation, and the flow it produces.
- Develop a model of the flow for assessing the probability of the onset of DDT.

To develop a physical understanding of the thermo-hydrodynamics of the flame, its propagation, and the flow it produces, we chose a model for the flame, physically interpreted the equations governing flame propagation, and derived the equations governing shock formation in the flow in front of an accelerating flame. To develop a model of the flow for assessing the probability of the onset of DDT, we constructed a solution for the unsteady flow produced by an accelerating flame and used its properties to establish conditions necessary for the onset of DDT.

A. Flames Treated as Reactive Discontinuities

It is convenient first to choose the simplest model and treat the flame as a reactive discontinuity. Implicit in this choice are the assumptions that the burning reaction is fast and that the hydrodynamic flow produced by an unsteady flame is not appreciably influenced by the detailed structure of the flame. In this case, states connected by the burning process are governed by the Rankine-Hugoniot jump conditions expressing the conservation of mass, momentum, and energy across the reactive discontinuity.

Let v denote specific volume; F, flame velocity; u, particle velocity; p, pressure; and h, specific enthalpy; and let the subscripts + and - denote the initial and final states, respectively connected by the flame. The states across the discontinuity are related by the Rankine-Hugoniot jump conditions[1]

$$v_-(F - u_+) = v_+(F - u_-) \tag{1}$$

$$(u_- - u_+)^2 = (p_- - p_+)\ (v_+ - v_-) \tag{2}$$

$$2(h_- - h_+) = (p_- - p_+)\ (v_- + v_+) \tag{3}$$

Equation (1) expresses the conservation of mass, Eq. (2) expresses the conservation of mass and momentum, and Eq. (3) expresses the conservation of mass, momentum, and energy. The locus of states attainable from a given initial state (p_+, v_+, h_+) lie on a curve in the (p,v) plane obtained by eliminating h between Eq. (3) and the $h = h(p,v)$ equation of state of the burnt products. This curve, called the Hugoniot curve centered on (p_+, v_+), has two branches when the discontinuity is reactive.

When the reaction is exothermic, the branch where $p_- > p_+$ and $v_- \leq v_+$ is called the detonation branch, and the branch where $p_- \leq p_+$ and $v_- > v_+$ is called the deflagration branch. With the present model of the flame, burnt states are represented by points on the deflagration branch of the Hugoniot curve. Moreover, the maximum flame speed is defined by the Chapman-Jouguet (CJ) point where $F = u_- + c_-$ (c denotes sound speed), the flow is sonic, and the Rayleigh line through the initial state (p_+, v_+),

$$p - p_+ = \left(\frac{F - u_+}{v_+}\right)^2 (v_+ - v) \tag{4}$$

is tangent to the Hugoniot curve.

Equations for deflagration CJ parameters will be derived, and then the differential equation governing the propagation of a reactive discontinuity will be formulated. Equation of state information must be specified to compute CJ parameters and states on the deflagration Hugoniot curve. Let the subscript o denote the standard state, and let the superscripts x and p denote propellant and propellant products, respectively. The initial enthalpy of the propellant and the $h = h^p(p,v)$ equation of state of the products are written as

$$h_+^x = \Delta H_o^x + h_+^x (p_+, v_+) \tag{5}$$

and

$$h^p = H_o^p + \frac{kpv}{k-1} \tag{6}$$

where $H_o^p = \Delta H_o^p - k\, p_o v_o/(k-1)$, ΔH_o denotes the heat of formation, and k denotes the polytropic index of propellant products. The combination of Eqs. (3) and (6) gives the equation for the Hugoniot curve centered on $(p_+ v_+)$ as

$$k\,(\mu v_- - v_+) + p_+(v_+ + v_-) = 2\,q \tag{7}$$

where $\mu = (k+1)/(k-1)$ and $q = [(\Delta H_o^x - \Delta H_o^p) + h^x(p_+, v_+) + k\, p_o v_o/k - 1]$.

At this stage it is convenient to neglect the $kp_o v_o/(k-1)$ term in q and introduce the nondimensional variables $p_-/p_+ = P$, $v_-/v_+ = V$, $q/p_+ v_+ = Q$ and $U^2 = (u_- - u_+)^2/p_+ v_+$. Equations (2) and (7) can then be written as

$$(P-1)\,(1-V) = U^2 \tag{8}$$

and

$$P(\mu V - 1) + (V+1) = 2Q \tag{9}$$

Using Eq. (4) and the definition of sound speed $c^2 = kpv$, the CJ condition $F - u_- = c_-$ can be written as

$$\frac{P-1}{1-V} = k\,\frac{P}{V} \tag{10}$$

The CJ parameters are obtained by solving Eqs. (8) - (10) and Eq. (1). The combination of Eqs. (8) - (10) leads to the following equations relating U and V to Q.

$$\mu U^2 + (\mu + 1) - 2Q = 0 \tag{11}$$

$$(1 - V)^2 + 2B(1 - V) - \left(\frac{\mu - 1}{\mu}\right)B = 0 \tag{12}$$

where $B = [2Q/(\mu + 1) - 1]$. The roots of Eqs. (11) and (12) give the particle velocities and volumes at the CJ points on the detonation and deflagration branches of the Hugoniot curve centered at (p_+, v_+). Solving Eq. (11) and converting back to dimensional variables gives the equation

$$u_- = u_+ \pm \frac{1}{k + 1}\left[2\{(k^2 - 1)q - k(k + 1)p_+v_+)\}\right]^{1/2} \tag{13}$$

where the positive sign gives the particle velocity at the CJ point on the detonation branch of the Hugoniot, and the negative sign gives the particle velocity at the CJ point on the deflagration branch.

Whereas liberation of chemical energy in a detonation produces mass motion directed toward the reaction front, the liberation of chemical energy in a deflagration produces mass motion directed away from the reaction front. Expanding the square root term in the equation for the roots of Eq. (12) gives the following equations for the CJ volumes on the detonation (14) and deflagration (15) branches as

$$\frac{v_-}{v_+} = \frac{k}{k + 1} \tag{14}$$

and

$$\frac{v_-}{v_+} = \frac{2(k - 1)Q}{k} - \frac{k}{k + 1} \tag{15}$$

Rearranging Eq. (1) to give the equation

$$F - u_+ = \frac{(u_- - u_+)}{(V - 1)} \tag{16}$$

and eliminating $(u_- - u_+)$ by using Eq. (13) with $A^2 = 2[(k^2 - 1)q - k(k + 1)p_+v_+]$ gives the equation for the maximum deflagration velocity as

$$F - u_+ = \frac{A}{(1 + A^2/kp_+v_+)} \tag{17}$$

The equation for the CJ deflagration pressure then follows from Eq. (9) as

$$P - 1 = -\frac{A^2/p_+v_+}{(k + 1)\ (1 + A^2/kp_+v_+)} \tag{18}$$

When $A^2/kp_+v_+ \gg 1$, Eq. (17) gives the maximum deflagration velocity as

$$F - u_+ = k\frac{p_+v_+}{A} \tag{19}$$

and the corresponding equation for the change in pressure across the discontinuity follows from Eq. (19) as

$$p_+ - p_- = \frac{kp_+}{k + 1} \tag{20}$$

Equations (13), (15), and (18) show that the reaction in a CJ deflagration wave produces a decrease in particle velocity and pressure but an increase in volume. Other states on the deflagration Hugoniot curve must be considered, however, because the CJ deflagration represents a hypothetical idealized case. These states lie on the weak deflagration branch where $p_{CJ} < p_- \leq p_+$, and where, according to Jouguet's rules, the flow of reaction products is subsonic with respect to the reaction front. Jouguet's rules for the flow in front of a weak deflagration give an insight into the problem of modeling unsteady deflagration and DDT. The flow ahead of the wave is influenced by the wave itself because the flow ahead of the wave is subsonic with respect to the wave front. Consequently, an accelerating flame produces an unsteady compression wave ahead of itself and the initial pressure for the burning process increases as the flow develops. The burnt states are represented by points on the family of deflagration Hugoniot curves centered on an adiabatic compression curve of unburnt material. Moreover, the continued acceleration of the flame will result in shock formation and initiation of detonation in material ahead of the flame front.

The differential equation governing the propagation of a reactive discontinuity will now be derived to obtain a more quantitative description of unsteady deflagration waves. Let t and x denote time and Eulerian distance, respectively, and $p_+ - p_- = \Delta p$ and $u_+ - u_- = \Delta u$. When the deflagration propagates as a discontinuity, the time variations of p_+ and p_- satisfy the equations

$$\frac{Dp_+}{Dt} = \frac{\partial p}{\partial t_+} + F \frac{\partial p}{\partial x_+} \tag{21}$$

$$\frac{Dp_-}{Dt} = \frac{\partial p}{\partial t_-} + F \frac{\partial p}{\partial x_-} \tag{22}$$

Where the subscripts + and - denote that the partial derivatives are evaluated at the top and bottom of the discontinuity (the initial and final states). Substracting Eqs. (21) and (22) after the partial time derivatives have been eliminated using the identity

$$\frac{dp}{dt} = \frac{\partial p}{\partial t} + u \frac{\partial p}{\partial x} \tag{23}$$

leads to the equation

$$\frac{D\Delta p}{Dt} = \frac{dp}{dt_+} - \frac{dp}{dt_-} + (F - u_+) \frac{\partial p}{\partial x_+} - (F - u_-) \frac{\partial p}{\partial x_-} \tag{24}$$

A similar procedure leads to the corresponding equation for u

$$\frac{D\Delta u}{Dt} = \frac{du}{dt_+} - \frac{du}{dt_-} + (F - u_+) \frac{\partial u}{\partial x_+} - (F - u_-) \frac{\partial u}{\partial x_-} \tag{25}$$

The equation governing the discontinuity is obtained by combining Eqs. (24) and (25) with the equations of motion, which are written as

$$\rho \frac{du}{dt} = - \frac{\partial p}{\partial x} \tag{26}$$

$$\frac{dp}{dt} = c^2 \frac{d\rho}{dt} = - c^2 \rho \frac{\partial u}{\partial x} \tag{27}$$

with $\rho = 1/v$ used to denote the density. Multiplying Eq. (25) by $\dot{M} = \rho_+(F - u_+) = \rho_-(F - u_-)$ and adding the resulting equation to Eq. (24) leads to the equation

$$\frac{D\Delta p}{Dt} + \dot{M} \frac{D\Delta u}{Dt} = - \rho_+[c_+^2 - (F - u_+)^2] \frac{\partial u}{\partial x_+} + \rho_-[c_-^2 - (F - u_-)^2] \frac{\partial u}{\partial x_-} \tag{28}$$

Equation (28) gives hydrodynamic conditions associated with deflagration waves. Consider first a deflagration wave propagating at constant velocity when $D(\Delta p)/\Delta t = D(\Delta u)/Dt = 0$ and both terms on the right-hand side of Eq. (28) are zero. Necessary conditions for this case are either $\partial u/\partial x_+ = \partial u/\partial x_- = 0$, or $\partial u/\partial x_+ = 0$ and $c_- = F - u_-$, because unreacted material satisfies the condition $c_+ > F - u_+$. Solutions involving a pre-compression shock followed by a deflagration wave can be constructed to satisfy both of these conditions. Rejection of the CJ condition on physical grounds, however, gives $\partial u/\partial x_+ = \partial u/\partial x_- = 0$ as the necessary hydrodynamic condition for steady deflagration waves. Of particular interest is the flow when the particle velocity of burnt material is zero. In this case the strength of the shock and deflagration waves are such that the increase in particle velocity produced by the shock is exactly offset by the decrease in particle velocity produced by the deflagration.

B. Shock Formation in Front of an Accelerating Flame

The factors governing shock formation in front of an accelerating flame were considered because formation of a shock is necessary for DDT. A shock is necessary for the onset of DDT because detonation is a shock supported by chemical reaction. At this stage in this report we will use the subscript o to denote the state in virgin material, rather than the standard state. With the notation already introduced for the variables, we let h and σ denote Lagrange distance and stress and write the equations of motion governing our one dimensional flow as

$$\left(\frac{\partial v}{\partial t}\right)_h = v_o \left(\frac{\partial u}{\partial h}\right)_t \tag{29}$$

$$\left(\frac{\partial u}{\partial t}\right)_h = - v_o \left(\frac{\partial \sigma}{\partial h}\right)_t \tag{30}$$

$$\left(\frac{\partial e}{\partial t}\right)_h = - \sigma \left(\frac{\partial v}{\partial t}\right)_h \tag{31}$$

It is convenient in considering shock formation to rewrite Eqs. (29) and (30) as

$$- v_o \left(\frac{\partial u}{\partial v}\right)_h = \left(\frac{\partial h}{\partial t}\right)_u = C_u \tag{32}$$

and

$$v_o \left(\frac{\partial \sigma}{\partial u}\right)_h = \left(\frac{\partial h}{\partial t}\right)_\sigma = C_\sigma \tag{33}$$

Equations (32) and (33) are also useful for the Lagrange analysis. The quantities C_u and C_σ are, respectively, the slopes of the curves of constant particle velocity and stress in the (t,h) plane. In other words, the points of constant particle velocity in a wave propagate at C_u and the points of constant stress propagate at C_σ. A shock will be formed in the compressive part of a wave when the wave profile steepens as the wave propagates. The conditions for compressive wave steepening, $(\partial C_u/\partial u)_h > 0$ and $(\partial C_\sigma/\partial \sigma)_h > 0$, are thus kinematic conditions for shock formation. These conditions are related to dynamic material properties by the following equations

$$\left(\frac{\partial C_u}{\partial u}\right)_h = - v_o \frac{(\partial^2 u/\partial v^2)_h}{(\partial u/\partial v)_h} \tag{34}$$

$$\left(\frac{\partial C_\sigma}{\partial \sigma}\right)_h = v_o \frac{(\partial^2\sigma/\partial u^2)_h}{(\partial\sigma/\partial u)_h} \tag{35}$$

obtained by differentiating Eq. (32) partially with respect to u and differentiating Eq. (33) partially with respect to σ. Because $(\partial u/\partial v)_h < 0$ and $(\partial\sigma/\partial u)_h > 0$ during compression, the dynamic material properties associated with shock formation follow readily from Eq. (34) and Eq. (35) as $(\partial^2 u/\partial v^2)_h > 0$ and $(\partial^2\sigma/\partial u^2)_h > 0$.

Properties of the Lagrange stress-strain curve associated with shock formation are obtained from the equation

$$\left(\frac{\partial\sigma}{\partial v}\right)_h = -\frac{C_\sigma C_u}{v_o^2} \tag{36}$$

obtained by combining Eqs. (32) and (33). Differentiation of Eq. (36) gives the equation

$$-v_o^2 \frac{(\partial^2\sigma/\partial v^2)_h}{(\partial\sigma/\partial v)_h} = v_o(\partial C_u/\partial u)_h + C_u(\partial C_\sigma/\partial\sigma)_h \tag{37}$$

The condition that the Lagrange (σ,v) relationship must satisfy for shock formation to occur in compression follows as $(\partial^2\sigma/\partial v^2)_h > 0$ because $(\partial\sigma/\partial v)_h < 0$.

We will now consider shock formation in a simple wave adjacent to a constant state. In a simple wave, the stress and specific volume are functions only of particle velocity[2] $C_\sigma = C_u$, and the curves of constant particle velocity, of constant stress, and of constant volume are straight lines. Equation (36) can then be written as

$$\left(\frac{\partial\sigma}{\partial v}\right)_h = -\left(\frac{C_\sigma}{v_o}\right)^2 = -\left(\frac{C_u}{v_o}\right)^2 \tag{38}$$

and differentiated to give the equations

$$-\frac{v_o}{2}\,\frac{(\partial^2\sigma/\partial v^2)_h}{(\partial\sigma/\partial v)_h} = \frac{C_\sigma}{v_o}\left(\frac{\partial C_\sigma}{\partial\sigma}\right)_h = \left(\frac{\partial C_u}{\partial u}\right)_h \tag{39}$$

These equations again show that the condition $(\partial^2\sigma/\partial v^2)_h > 0$ must be satisfied for shock formation. In classical work[1], simple waves are treated in terms of characteristic curves. The differential equation for the characteristic curves is

$$\frac{dh}{dt} = \pm\,\frac{v_o c}{v} \tag{40}$$

where the sound speed c is defined by the identity $(c/v)^2 = -(\partial p/\partial v)_s$ and where s denotes entropy and p denotes pressure. The characteristics associated with the plus sign are called C_+ characteristics and those associated with the minus sign are called C_- characteristics. At this stage we identify the stress with the pressure, set $\sigma = p$ accordingly, and use the $e = e(s,v)$ equation of state to rewrite Eq. (31) as

$$\left(\frac{\partial s}{\partial t}\right)_h = 0 \tag{41}$$

It then follows from Eq. (36), Eq. (41), and the identity

$$\left(\frac{\partial p}{\partial v}\right)_h = \left(\frac{\partial p}{\partial v}\right)_s + \left(\frac{\partial p}{\partial s}\right)_v \left(\frac{\partial s}{\partial t}\right)_h \tag{42}$$

that

$$-\left(\frac{\partial p}{\partial v}\right)_h = \frac{C_p C_u}{v_o^2} = \frac{c^2}{v^2} \tag{43}$$

Equation (40) for the simple wave can then be written as

$$\frac{dh}{dt} = \pm C_u \tag{44}$$

and it follows that the characteristics coincide with the curves of constant particle velocity and are straight lines.

We will now consider shock formation in a simple wave produced by an accelerating piston or an accelerating flame. A shock is formed where the forward facing characteristics emanating from the piston or the flame intersect to form an envelope. Integrating Eq. (44) gives the particle velocity field for the flow produced by a piston as

$$h = C_u[t - t_p(u)] \tag{45}$$

where the subscript P denotes the piston, and gives the particle velocity field for the flow produced by the flame as

$$h = h_f(u) + C_u[t - t_f(u)] \tag{46}$$

where the subscript f denotes the flame discontinuity.

The condition that the derivative $(\partial h/\partial u)_t$ vanishes on the envelope formed by the characteristics gives the parametric representation of this envelope as

$$t_e = t_p(u) + \frac{C_u}{(du_p/dt)(dC_u/du)} \tag{47}$$

and

$$h_e = \frac{C_u^2}{(du_p/dt)(dC_u/du)} \tag{48}$$

where $(u \quad du) = -v_o(\partial^2 p/\partial v^2)_s/2(\partial p/\partial v)_s$. Equations (47) and (48) show that the C_+ characteristics emanating from an accelerating piston $du_p/dt > 0$ form an envelope in front of the piston $h_p = 0$ when $(\partial^2 p/\partial v^2)_s > 0$. Let the subscript i denote the initial condition at the origin. When $(du_p/dt)_i > 0$, the shock is formed at the point $t = t_c$, $h = c_o t_c$ on the C_+ characteristic through the origin; t_c is given by Eq. (47) as

$$t_c = \frac{c_o}{(du_p/dt)_i (dC_u/du)_i} \tag{49}$$

The parametric representation of the envelope associated with an accelerating flame is obtained from Eq. (46) as

$$t_e = t_f(u) + \frac{(C_u - dh_f/dt)}{(du_-/dt)(dC_u/du)} \tag{50}$$

and

$$h_e = h_f(u) + C_u \frac{(C_u - dh_f/dt)}{(du_-/dt)(dC_u/du)} \tag{51}$$

We consider a flame with an initial velocity $(dh_f/dt)_i = 0$ but with an initial acceleration $(du_-/dt)_i > 0$. In this case, as with the accelerating piston, the shock is formed at the point $t = t_c$, $h = c_o t_c$ on the C_+ characteristic through the origin; the time t_c is given by

$$t_c = \frac{c_o}{(du_-/dt)_i (dC_u/du)_i} \tag{52}$$

from Eq. (50).

It is clear, in contrast to the case of the accelerating piston, that there is a class of accelerating flames that is associated with shock formation and a class that is not. These classes are separated by the accelerating flame that overtakes the first characteristic at the time t_c. A shock is formed by accelerating flames that would overtake the first characteristic after t_c, but a shock is not formed by accelerating flames that overtake the first characteristic before t_c.

C. Model Solution for Assessing the Probability of the Onset of DDT

Our model solution is based on the assumption that the following chain of events is responsible for DDT in burning propellant contained in a closed tube

- The formation of an accelerating flame by an unsteady burning process.
- The formation of a shock wave in unburnt material by the compressive action of the accelerating flame in the deflagration to shock transition.
- The formation of a detonation wave in material ahead of the flame by the shock to detonation transition SDT.

In this case, DDT will not occur unless the accelerating flame produces a shock wave, and the properties of this shock satisfy the conditions required for the occurrence of SDT. The condition for shock formation is thus not a criticality condition for DDT, and the shock must be characterized to assess the probability of DDT.

Our analytical treatment of DDT is based on the premise that the dynamics of the flow behind and in front of the accelerating flame must be considered to characterize the shock formed in front of the flame and to assess the probability of DDT. It is therefore necessary to model the accelerating flame and the unsteady flows on both sides of it. The model for these unsteady processes used here is based on the model formulated by Jones[3] to investigate the DDT process in gases. We treat the flame as a reactive discontinuity, we treat the flow in front of the flame as a simple compression wave, and we assume that the density gradient is zero in the flow behind the flame. The one-dimensional differential equations governing this type of flow in a closed tube can be solved when relationships for

the burning rate and the acceleration of the flame are known. This treatment is phenomenological but supersedes previous thermo-hydrodynamic treatments[4-6] by making the states attained across the flame compatible with the differential equations governing the conservation of mass and momentum in the flow behind the flame, and by making the states compatible with the rear-boundary particle velocity condition in the closed tube.

It is convenient in constructing solutions for such flows to extend the notation introduced on page 8. We will still use f as a superscript or subscript to denote the flame discontinuity, but we now use the subscripts + and - to denote quantities in front of the flame discontinuity and behind it. States across the flame are then related by the Rankine-Hugoniot jump conditions written as

$$\rho_+^f (F - u_+^f) = \rho_-^f (F - u_-^f) \tag{53}$$

$$p_+^f - p_-^f = \rho_+^f (F - u_+^f) (u_+^f - u_-^f) \tag{54}$$

$$2(e_-^f - e_+^f) = (p_+^f + p_-^f) (v_+^f - v_-^f) \tag{55}$$

Again, we let c denote the sound speed and the subscript o denote the initial state in the propellant. We also assume that the propellant is governed by a Murnaghan equation with an index n = 3. The equations for p_+, ρ_+, e_+, and the slope of a forward facing C_+ characteristic $(u_+ + c_+)$ in simple isentropic compression wave can then be written as

$$p_+ = \frac{c_o^2 \rho_o}{3} \left[\left(1 + \frac{u_+}{c_o} \right)^3 - 1 \right] + p_o \tag{56}$$

$$\rho_+ = \rho_o \left(1 + \frac{u_+}{c_o} \right) \tag{57}$$

$$e_+ = e_o + \frac{(p_+ - p_o)v_+}{2} + \frac{(\rho_o c_o^2 - 2p_o)}{2}(v_+ - v_o) \tag{58}$$

$$u_+ + c_+ = c_o + 2u_+ \tag{59}$$

We denote the extent and heat of reaction by λ and q, assume that the reaction products are polytropic with an index k = 3, and write the equation of state for material behind the flame as

$$e_- = e_o - \lambda q + \frac{(pv)}{2} - \frac{\lambda p_o v_o^p}{2} - (1 - \lambda)\frac{p_o v_+(p_-)}{2}$$

$$+ (1 - \lambda)\frac{(c_o^2 \rho_o - 2p_o)}{2}(v_+(p_-) - v_o) \tag{60}$$

where $v_+(p_-)$ is written to denote that the volume of the propellant is related to the pressure by the same equation on both side of the flame, and v_o^p denotes the specific volume of the reaction products in their standard state. Combining Eq. (55), (58), and (60) allows us to write the extent of reaction in the flame as

$$\lambda^f = \Delta E^f / Q^f \tag{61}$$

where

$$Q^f = [2q + p_o(v_o^p - v_o) + (c_o^2\rho_o - 3p_o)(v_+(p_-^f) - v_o)] \tag{61a}$$

and

$$\Delta E^f = [(p_- + p_+)(v_- - v_+) + (pv)_- - (pv)_+$$

$$+(c_o^2\rho_o - 3p_o)(v_+(p_-) - v_o)]^f \tag{61b}$$

with f written as a superscript outside the bracket for notational convenience.

With x and t used to denote Eulerian distance and time, we set $F = dx^f/dt$. In contrast to Jones[3] we assume that the burning rate is related to the particle velocity and the pressure at the flame front by the equation

$$F = u_+^f + A(p_+^f - p_o) \tag{62}$$

where A is the burning rate parameter. The assumption that the pressure exponent in Eq. (62) is 1 is not necessary, but is made here for convenience.

We are now in a position to consider the flow produced in a closed tube by a flame that is treated as a reactive discontinuity. We will first derive equations for the initial conditions attained in the tube and then present solutions for flows produced by flames with different types of acceleration.

1. Initial Conditions Produced by the Propagation of a Flame in a Closed Tube

The flow produced by the propagation of a deflagration wave from a rigid wall is of particular interest because our experimental study of DDT is designed to model this rear-boundary condition. We use r as a subscript and as a superscript to denote the rear-boundary and we use the subscript i to denote initial values of quantities at time t = 0.

The rear-boundary condition for the particle velocity at the wall is expressed by the equation

$$u_-^r = 0 \tag{63}$$

Because $(u_+^f)_i = 0$ and $(p_+^f)_i = p_o$, it follows from Eq. (62) that $F_i = 0$. In this case $(u_-^f)_i = (u_-^r)_i$, and it follows from Eq. (63) that $(u_-^f)_i = 0$. Differentiating Eq. (63) twice with respect to time leads to the conditions $du_-^r/dt = d^2u_-^r/dt^2 = 0$ and it follows from the identities

$$\frac{du_-^r}{dt} = \frac{\partial u_-}{\partial t_r} + u_-^r \frac{\partial u_-}{\partial x_r} \tag{64}$$

and

$$\frac{d^2 u_-^r}{dt^2} = \frac{\partial^2 u_-}{\partial t_r^2} + 2u_-^r \frac{\partial^2 u_-}{\partial t \partial x_r} + (u_-^r)^2 \frac{\partial^2 u_-}{\partial x_r^2} + \frac{du_-^r}{dt} \frac{\partial u_-}{\partial x_r} \tag{65}$$

that $(\partial u_-/\partial t)_r = (\partial^2 u_-/\partial t^2)_r = 0$, and thus that $(\partial u_-/\partial t)_i = (\partial^2 u_-/\partial t^2)_i = 0$. We now use the following identities for the time derivatives of u_-^f along the flame path,

$$\frac{Du_-^f}{Dt} = \frac{\partial u_-}{\partial t_f} + F \frac{\partial u_-}{\partial x_f} \tag{66}$$

$$\frac{D^2 u_-^f}{Dt^2} = \frac{\partial^2 u_-}{\partial t^2}_f + 2F \frac{\partial^2 u_-}{\partial t \partial x}_f + F^2 \frac{\partial^2 u_-}{\partial x^2}_f + \frac{dF}{dt} \frac{\partial u_-}{\partial x}_f \tag{67}$$

to derive an equation for the initial value of the particle velocity gradient behind the flame. It follows from equation (66) that $(Du_-^f/Dt)_i = 0$ because $(\partial u_-/\partial t)_i = 0$ from Eq. (64) and $F = 0$ from Eq. (62). In this case, Eq. (67) gives the equation for $(\partial u_-/\partial x)_i$ as

$$\left(\frac{D^2 u_-^f}{Dt^2}\right)_i = \frac{dF}{dt_i} \left(\frac{\partial u_-}{\partial x}\right)_i \tag{68}$$

because $(\partial^2 u_-/\partial t^2)_i = 0$ from Eq. (65). It follows from Eq. (68) that $(D^2 u_-^f/Dt^2)_i$ and $(\partial u_-/\partial x)_i$ have the same sign because $dF/dt_i > 0$ is the initial condition for the flame to propagate along the tube.

We now use the conservation of mass expressed by Eq. (53) to calculate the initial density behind the flame and show that the flame produces a compression wave in virgin material as it propagates from the wall. Setting $F_i = (u_+^f)_i = (u_-^f)_i = 0$ and $(Du_-^f/Dt)_i = 0$ in the equation obtained by differentiating Eq. (53) with respect to time leads to the following equations for the initial density behind the flame:

$$(\rho_-^f)_i = \rho_o \left[\frac{(DF/Dt)_i - (Du_+^f/Dt)_i}{(DF/t)_i}\right] \tag{69a}$$

and

$$(\rho_-^f)_i = \rho_o \left[\frac{(DF/Du_+^f)_i - 1}{(DF/Du_+^f)_i}\right] \tag{69b}$$

Because $(DF/Du_+^f)_i > 0$ it follows from Eq. (69b) that $(\rho_-^f)_i < \rho_o$, and it then follows from Eq. (69a) that $(Du_+^f/Dt)_i > 0$. It then follows from the identity

$$\frac{Du_+^f}{Dt} = \frac{du_+^f}{dt} + (F - u_+^f)\frac{\partial u_+}{\partial x_f} \tag{70}$$

that $(du_+^f/dt)_i = (Du_+^f/Dt)_i > 0$. Thus the particle velocity at the flame front starts to increase and the deflagration starts to produce a compressive wave ahead of itself.

The equation for the initial value of the particle velocity gradient behind the flame is obtained by combining Eq. (68) with the equation obtained by differentiating Eq. (53) twice with respect to time, and making use of the continuity equation and the equations expressing the rear-boundary conditions. After some manipulation the equation for $(\partial u_-/\partial x)_i$ can be written as

$$\left(\frac{\partial u_-}{\partial x}\right)_i = -\frac{\left(\frac{Du_+^f}{Dt}\right)_i}{3}\left\{\frac{2\left(\frac{d\tilde{\rho}_+}{du_+}\right)_i\left[\left(\frac{DF}{Du_+^f}\right)_i - 1\right] + \left(\frac{D^2F_2}{Du_+^f}\right)\Big/\left(\frac{DF}{Du_+^f}\right)_i}{\left(\frac{DF}{Du_+^f}\right)_i - 1}\right\} \tag{71}$$

where $\tilde{\rho}_+$ is defined by the equation $\rho_+ = \rho_o\tilde{\rho}_+$. It follows from Eq. (71) that $(\partial u_-/\partial x)_i < 0$ in a closed tube because the term in braces > 0 and $(Du_+^f/Dt)_i > 0$. Thus the flow starts to develop with negative particle

velocity behind the flame. In the case when F satisfied equation (62) and p_+ and ρ_+ satisfy Eq. (56) and (57), the initial value of the particle velocity gradient behind the flame is given by the equation

$$\left(\frac{\partial u_-}{\partial x}\right)_i = -\frac{2}{3}\,\frac{(Du_+^f/Dt)_i}{c_o}\left[\frac{A\rho_o c_o + 1}{A\rho_o c_o}\right] \tag{72}$$

Equations for the pressure are readily obtained from Eq. (54) written as

$$p_+^f - p_-^f = \dot{M}\,(u_+^f - u_-^f) \tag{73}$$

with $\dot{M} = \rho_+^f\,(F - u_+^f)$. Differentiating Eq. (73) and imposing the rear-boundary conditions leads to the equation

$$\left(\frac{Dp_+^f}{Dt}\right)_i = \left(\frac{Dp_-^f}{Dt}\right)_i \tag{74}$$

It follows from the identities

$$\frac{Dp_+^f}{Dt} = \frac{dp_+}{dt_f} + (F - u_+^f)\,\frac{\partial p_+}{\partial x_f} \tag{75}$$

$$\frac{Dp_-^f}{Dt} = \frac{dp_-}{dt_f} + (F - u_-^f)\,\frac{\partial p_-}{\partial x_f} \tag{76}$$

that $(Dp_+^f/Dt)_i = (dp_+/dt)_i = (Dp_-^f/Dt)_i = (dp_-/dt)_i$. The isentropic condition $dp_+ = \rho_+ c_+ du_+$ can then be written at $t = 0$ as

$$\frac{Dp_+^f}{Dt_i} = \rho_o c_o\,\frac{Du_+^f}{Dt_i} \tag{77}$$

and combined with Eq. (69) to obtain the equation

$$\left(\frac{dp_+}{dt}\right)_i = \left(\frac{dp_-}{dt}\right)_i = c_o\,[\rho_o - (\rho_-^f)_i]\left(\frac{dF}{dt}\right)_i \tag{78}$$

which shows that the pressure starts to increase behind and in front of the flame as the flame starts to propagate down the tube. The combination of the energy equation, $dp_+/dt = -\rho_+ c_+^2\,(\partial u_+/\partial x)$, evaluated at $t = 0$ with Eq. (78) then gives the equation for the initial value of the particle velocity gradient in front of the flame as

$$\left(\frac{\partial u_+}{\partial x}\right)_i = -\frac{[\rho_o - (\rho_-^f)_i]}{\rho_o c_o}\left(\frac{DF}{Dt}\right)_i \tag{79}$$

Because $\rho_o > (\rho_-^f)_i$, Eq. (79) shows that the initial value of the particle velocity gradient in front of the flame is also negative.

Differentiating Eq. (73) twice with respect to time and imposing the initial and rear-boundary conditions leads to the equation

$$\left[\frac{D^2(p_+^f - p_-^f)}{Dt^2}\right]_i = 2\rho_o\left[\left(\frac{DF}{Du_+^f}\right)_i - 1\right]\left(\frac{Du_+^f}{Dt}\right)_i^2 \tag{80}$$

Equation (80) shows that the pressure difference across the flame initially increases as the flow develops.

2. Flames with u_+^f Governed by a Power Law

The solution with the particle velocity at the flame front u_+^f governed by a power law of the form

$$u_+^f = \alpha_m t^m \tag{81}$$

with α_m and m considered as parameters was presented at the Seventh Symposium (International) on Detonation held from June 16-19, 1981 at the United States Naval Academy, Annapolis, Maryland. Only a brief account of this solution is given here (the paper presented at the symposium is included as the Appendix at the end of this report).

Expressions for the burning rate and acceleration of the flame given by Eqs. (62) and (81) were used to construct a model solution for the flow produced by an unsteady flame propagating in a closed tube. Equations for the time the shock is formed in front of the flame were derived, and a graphical method[7], based on the particle velocity profiles, was used to determine the strength and position of the shock at later times. The Hugoniot equation, Eq. (55) and the equation of state Eq. (60) were used to calculate the time t_R taken for the reaction to procede to completion in the flame discontinuity. The time t_R defines the time interval $0 \leq t \leq t_R$ over which Eq. (81) can be used to describe the acceleration of the flame. Consideration of the evolution of the shock preceding the flame after the time t_R let to the postulate that the pressure attained at the flame front when the reaction proceeds to completion in the flame can be used to assess the probability of the occurrence of DDT. Examination of particular solutions in the light of this postulate led to the conclusion that DDT depends strongly on the burning rate and will probably not occur unless the burning rate parameter A exceeds a critical value.

3. Flames Attaining a Constant Velocity $\hat{F}$

For the sake of tractability, the model solution for flames attaining a constant velocity was based on the following equation governing the acceleration of the flame,

$$\frac{dt}{du_+^f} = \frac{\alpha}{c_o^2} (\hat{u}_+^f - u_+^f) \tag{82}$$

where α denotes a characteristic time and $\hat{u}_+^f$ is the particle velocity at the flame front at the time $t = \hat{t}$ when $F = \hat{F}$. The equation for the

variation of the particle velocity u_+^f with respect to time is readily obtained as

$$t = \hat{t} - \frac{\alpha}{2c_o^2}\left(\hat{u}_+^f - u_+^f\right)^2 \tag{83}$$

with $\hat{t} = (\alpha/2)(\hat{u}_+^f/c_o)^2$, by integrating Eq. (82) and setting $t = \hat{t}$ when $u_+^f = \hat{u}_+^f$.

Our model solutions are also based on the assumption that the flame attains its constant velocity $\hat{F}$ at the time $\hat{t} = t_R$, when the reaction is complete in the flame discontinuity, and thereafter propagates at $\hat{F}$. In this case, the condition, $u_+^f = \hat{u}_+^f$ when $\lambda^f = 1$, can be used to determine the values of $\hat{u}_+^f$, $\hat{F}$, and $\hat{t}$ associated with a prescribed value of the burning rate parameter A.

We will now derive the equations governing the flame trajectory and the states attained behind the flame. It is convenient to denote the equations in the paper in the Appendix by the letter A. It follows from Eqs. (A16), (A17), and (82) that the differential equation governing the flame trajectory can be written as

$$\frac{dx_f}{du_+^f} = \frac{\alpha B}{c_o^2}\left[D\left(\frac{u_+^f}{c_o}\right) + 3\left(\frac{u_+^f}{c_o}\right)^2 + \left(\frac{u_+^f}{c_o}\right)^3\right](\hat{u}_+^f - u_+^f) \tag{84}$$

where $D = 3 + c_o/B$ and $B = Ac_o^2\rho_o/3$. Integration of the terms obtained by expanding the right hand side of equation (84) allows us to write the equation for the flame trajectory as

$$x_f = I_1 - I_2 \tag{85}$$

with

$$I_1 = \alpha\beta\left(\frac{\hat{u}_+^f}{c_o}\right)\left(\frac{u_+^f}{c_o}\right)^2\left[\frac{D}{2} + \left(\frac{u_+^f}{c_o}\right) + \frac{1}{4}\left(\frac{u_+^f}{c_o}\right)^2\right] \tag{86}$$

and

$$I_2 = \alpha\beta\left(\frac{u_+^f}{c_o}\right)^3\left[\frac{D}{3} + \frac{3}{4}\left(\frac{u_+^f}{c_o}\right) + \frac{1}{5}\left(\frac{u_+^f}{c_o}\right)^2\right] \tag{87}$$

Setting $u_+^f = \hat{u}_+^f$ in Eqs. (85), (86), and (87) gives the distance taken for the flame to attain the constant velocity $\hat{F}$ as

$$\hat{x}_f = \frac{\alpha\beta}{2}\left(\frac{\hat{u}_+^f}{c_o}\right)^3\left[\frac{D}{3} + \frac{1}{2}\left(\frac{\hat{u}_+^f}{c_o}\right) + \frac{1}{10}\left(\frac{\hat{u}_+^f}{c_o}\right)^2\right] \tag{88}$$

Again the calculation of states behind the flame is based on the assumption that $(\partial\rho_-/\partial x) = 0$. In this case, the mass behind the flame can be written simply as $\rho_- x^f$, and formulation of the conservation of mass for the material that has passed through the flame front leads to the following equation for $\rho_- x^f$

$$\rho_- x^f = \int_0^{u_+^f} \rho_+^f (F - u_+^f)\ \frac{dt}{du_+^f}\ du_+^f \tag{89}$$

Because $\rho_- = \rho_-^f$, the density calculated from Eq. (89) can be used to calculate u_-^f and p_-^f from the jump conditions, Eqs. (53) and (54), and these quantities can be used to complete the characterization of the $u_-(x,t)$ and $p_-(x,t)$ fields behind the flame. We set $\dot{M}(u_+^f) = \rho_+^f(F - u_+^f)$ for convenience, and use Eqs. (62), (56), and (57) to obtain the following expression for $\dot{M}(u_+^f)$ in terms of u_+^f,

$$\dot{M}(u_+^f) = \rho_o B \left(\frac{u_+^f}{c_o}\right)\left[3 + 6\left(\frac{u_+^f}{c_o}\right) + 4\left(\frac{u_+^f}{c_o}\right)^2 + \left(\frac{u_+^f}{c_o}\right)^3\right] \tag{90}$$

It is convenient after performing the integration in Eq. (89) with Eq. (82) and (90) to write the equation for $\rho_- x^f$ as

$$\rho_- x^f = G_1 - G_2 \tag{91}$$

with

$$G_1 = \rho_o B\alpha\left(\frac{\hat{u}_+^f}{c_o}\right)\left(\frac{u_+^f}{c_o}\right)^2\left[\frac{3}{2} + 2\left(\frac{u_+^f}{c_o}\right) + \left(\frac{u_+^f}{c_o}\right)^2 + \frac{1}{5}\left(\frac{u_+^f}{c_o}\right)^3\right] \tag{92}$$

and

$$G_2 = \rho_o B\alpha\left(\frac{u_+^f}{c_o}\right)^3\left[1 + \frac{3}{2}\left(\frac{u_+^f}{c_o}\right) + \frac{4}{5}\left(\frac{u_+^f}{c_o}\right)^2 + \frac{1}{6}\left(\frac{u_+^f}{c_o}\right)^3\right] \tag{93}$$

The equation for the density $\hat{\rho}_-$ when the flame attains the constant velocity $\hat{F}$ is readily obtained from Eqs. (91)-(93) as

$$\hat{\rho}_- \hat{x}_f = \rho_o \frac{B\alpha}{2}\left(\frac{\hat{u}_+^f}{co}\right)^3\left[1 + \left(\frac{\hat{u}_+^f}{c_o}\right) + \frac{2}{5}\left(\frac{\hat{u}_+^f}{c_o}\right)^2 + \frac{1}{15}\left(\frac{\hat{u}_+^f}{c_o}\right)^3\right] \tag{94}$$

and combining Eq. (88) and Eq. (94) gives the corresponding equation for ρ_- as

$$\rho_- = \rho_o \frac{1 + (\hat{u}_+^f/c_o) + 2/5\ (\hat{u}_+^f/c_o)^2 + 1/15\ (\hat{u}_+^f/c_o)^3}{D/3 + 1/2\ (\hat{u}_+^f/c_o) + 1/10\ (\hat{u}_+^f/c_o)^2} \tag{95}$$

We are now in a position to construct particular model solutions for flames attaining a constant propagation velocity. Values of the input parameters used to generate these solutions are $\rho_o = 1.6$ g/cc, $c_o = 2$ mm/μs, $q = 54.69$ kbar cc/g, $v_o^p = 8.4 \times 10^{2}$ cc/g, $\alpha = 10^3$ μs, $p_o = 1 \times 10^{-3}$ kbar, and values of the burning rate parameter A in the range 1×10^{-3} - 1.2×10^{-2} mm/μs kbar. Equations (95), A29), (61), (61a) and (61b) and the condition $u_+^f = \hat{u}_+^f$, when $\lambda^f = 1$, were used to calculate values of $\hat{u}_+^f$ for the prescribed values of the burning rate parameter A, and the corresponding values of $\hat{p}_+^f$ were used to assess the probability of the occurrence of SDT. For values of u_+^f in the range $0 \leq u_+^f \leq \hat{u}_+^f$, the flame trajectory was calculated from Eqs. (85)-(87), and the states connected by the flame were calculated from Eqs. (85)-(87), (91)-(93), (A28),(A29), (61a), and (61b). Values of $\hat{t}$, $\hat{u}_+^f$, $\hat{u}_-^f$, $\hat{p}_+^f$, and $\hat{p}_-^f$ calculated with different values of the burning parameter are given in Table 1.

Table 1

$\hat{t}$, $\hat{u}_+^f$, $\hat{u}_-^f$, $\hat{p}_+^f$, $\hat{p}_-^f$

CALCULATED FOR VALUES OF THE BURNING RATE PARAMETER A

	$\hat{t}$	$\hat{u}_+^f$	$\hat{u}_-^f$	$\hat{p}_+^f$	$\hat{p}_-^f$
mm/μs kbar	μs	mm/μs	mm/μs	kbar	kbar
5.5×10^{-3}	10.1	0.284	-0.043	10.4	10.1
1.0×10^{-2}	44.4	0.596	-0.205	25.3	21.1
1.2×10^{-2}	80.2	0.801	-0.381	44.4	25.4

Examination of Table 1 shows that the values of the shock pressures $\hat{p}_+^f$ for assessing the probability of DDT for the values of the burning rate parameter, 5.0×10^{-3}, 1.0×10^{-2}, and 1.2×10^{-2} mm/μs kbar, are respectively 10.4, 25.3, and 44.4 kbar. DDT is expected to occur when the shock pressure $\hat{p}_+^f$ produced by the flame is 44.4 kbar and perhaps when $\hat{p}_+^f = 25.3$ kbar, but not when $\hat{p}_+^f = 10.4$ kbar. Here again, as in the calculation presented in the Appendix, the dependence of $\hat{p}_+^f$ on A shows

that the probability of DDT depends strongly on the burning rate parameter, and also leads to the conclusion that DDT will probably not occur in a closed tube when $A < 0.9 \times 10^{-3}$ mm/μs.

Theoretical Results and Conclusions

Equations governing flames treated as reactive discontinuities were derived and physically interpreted.

Conditions for shock formation were established, and the compressive flows produced by an accelerating flame and by an accelerating piston were compared to provide a better physical understanding of the compressive action of an accelerating flame.

Solutions describing the one-dimensional unsteady flow produced when an accelerating flame in a propellant or explosive contained in a closed tube attains a constant propagation velocity were constructed to model DST and gain an insight into DDT. The flame was treated as a reactive discontinuity, the flow in front of the flame was treated as a simple compression wave, and the density gradient was assumed to be zero in the flow behind the flame. The description of the flow is phenomenological because the burning rate, the acceleration of the flame, and the density gradient behind the flame must be prescribed to construct the solution. But this treatment supersedes previous thermodynamic treatments by accounting for the flow behind the flame as well as for the flow in front of it. Particular solutions were constructed for different values of the burning rate parameter A. The value of the pressure at the flame front $\hat{p}_+^f$ when the flame attained its constant propagation velocity after the time $\hat{t}$ was used to assess the probability of the occurrence of DDT. The dependence of $\hat{p}_+^f$ on A shows that DDT depends strongly on the burning rate and will probably not occur unless the burning rate parameter exceeds a value of approximately 1.0×10^{-2} mm/μs kbar.

The model solutions presented in this report for the flow associated with an accelerating reactive flame discontinuity provide guidelines for assessing the probability of the occurrence of DDT in a burning propellant contained in a closed tube. Questions regarding the applicability of

these solutions to real systems must be considered, however, because the extent of reaction in the flame discontinuity increases as the flow develops. In this case, the global assumptions made to model the flow may be reasonable for composite propellant containing components with markedly different reaction rates.

A more fundamental theoretical study of the flow produced by an unsteady flame must be undertake to obtain a more basic understanding of DDT. Questions regarding the treatment of a flame as a reactive discontinuity and the application of a steady-state burning rate expression to an unsteady flame must be addressed in this study, and a more realistic model must be developed for predicting the trajectory of the unsteady flame and the flow fields it produces.

III EXPERIMENTAL WORK

Initially the experimental studies were delayed because we could not find a source of propellant for the Lagrange gage experiments. Protracted negotiations to obtain HMX-based propellant for the DDT experiments from Lawrence Livermore National Laboratory LLNL were unsuccessful for the following reasons:

- Propellant was in short supply.
- The machining costs and times to meet tolerances in the dimensions of propellant samples (needed to construct the DDT gage assemblies) were prohibitive.

We subsequently found a source of HMX propellant at Edwards Air Force Base (EAFB), and personnel there agreed to provide the propellant required for this program. After discussions with EAFB personnel, we concluded that the usual method of constructing targets for Lagrange gage experiments from machined pieces was not practical for HMX-based propellants. Hence, an assembly based on casting rather than machining the propellant was designed to eliminate the complex machining and grooving operations conventionally used in constructing targets for Lagrange gage experiments. Assemblies consisting of acrylic tubes containing the stress gages and ionization pins were constructed and sent to EAFB to be filled with propellant. A gas gun experiment with Lagrange stress gages embedded in a propellant sample obtained from LLNL was also performed to test the gage configurations in the DDT experiments. The pressure histories recorded in this experiment validated the use of the gages in the configurations designed for the DDT experiments. DDT experiments with the filled assemblies obtained from EAFB were performed in steel and Lexan* tubes to:

- Record stress-time profiles in a propellant as it underwent the transition from deflagration to detonation.
- Measure flame trajectories in propellants undergoing DDT.

*Lexan is the trade name for polycarbonate manufactured by General Electric Co.

The experiments performed in steel tubes will be presented, followed by those performed in Lexan tubes.

A. Experiments in Steel Tubes

The experimental arrangement is shown in Fig. 1. It consisted of a thick-walled steel confinement tube, end plugs, an igniter cup, a PMMA tube containing the propellant and stress gages, and bolts and nuts to clamp the end plugs tightly to the confinement tube. The experimental arrangement will now be presented in more detail.

1. DDT Confinement Tube

The confinement tube was made of 4142 steel. It was 28 in. long with an inside diameter of 3 in. and an outside diameter of 7 in. The confinement tube, end plugs, and clamping bolts were designed to confine the high gas pressures, which were generated by the igniter and by the burning propellant, until pressures of the order of thousands of bars were reached. The inside diameter of the tube was large enough to make any diameter effect on burning negligible and large enough to exceed the critical diameter of the propellant. The end plug at the igniter end had a hole through which the igniter leads were passed.

2. Igniter

The igniter material was a mixture of boron and potassium nitrate with a laminac-lubersol binder obrained from Polytechnic Specialties in Byron, Georgia. The mixture was 22.7% boron, 71.7% potassium nitrate, and 5.6% binder. This mixture generates about 1600 cal/g of material. About 10 g of the igniter powder was placed in a Lucite cup lined on the bottom with a nichrome heating ribbon. The cup had an inside diameter of 2.5 in. and a depth of 0.25 in. The nichrome ribbon was about 11 in. long, 0.06 in. wide, and 0.007 in. thick; it had a resistance of about 1 ohm.

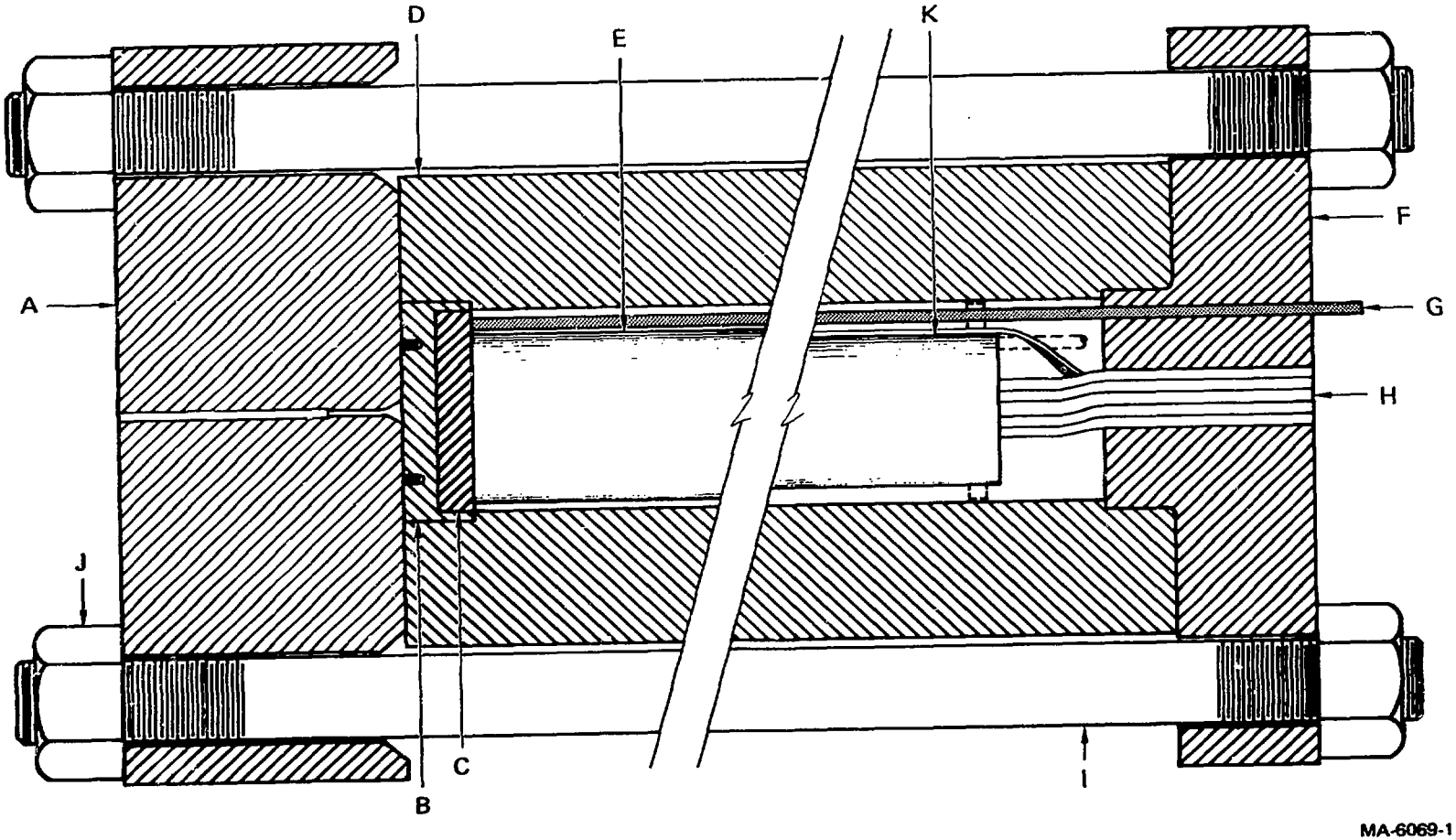

FIGURE 1 SCHEMATIC DRAWING OF EXPERIMENTAL ARRANGEMENT IN STEEL CONFINEMENT

A — Igniter end plug; B — Igniter cup holder; C — Igniter; D — steel DDT confinement cylinder; E — tube containing propellant; F — End plug; G — Light pipe; H — Leads from stress gages and ionization pins; I — High strength bolts; J — Nuts; K — Backing tube containing gage leads and epoxy. All regions within the DDT tube shown as voids are filled with epoxy.

The igniter material was thermally initiated using a 28 V, 5 A., dc power supply to actuate the nichrome heating ribbon.

3. Propellant Tube and Propellant

The Lucite tube used to contain the propellant inside the steel DDT tube is shown in Fig. 2 as it appears before the propellant is poured into it. This tube is a casting mold for the propellant and a jig for holding the gages during casting. The main section of the Lucite tube is 10 in. long and has an inside diameter of 2 in. This section was slit lengthwise down the center of the cylinder to support the gages. Three ytterbium stress gages were glued to a sheet of Kapton,* their leads insulated from one another by additional pieces of Kapton. The resulting Kapton sheet with gages was then glued between the two Lucite half cylinders, as shown in Fig. 2. The stress gages were located 1, 2, and 3 in. from the end of the cylinder. The gage leads were attached to Twinax† coaxial cable and potted with epoxy inside a Lucite backing tube that had an outside diameter of 2.25 in. (Fig. 2). The backing tube was to delay the arrival at the measuring stations of stress waves reflected from the end of the DDT tube. The entire assembly, propellant and backing tube, was 22.375 in. long. Three ionization pins were placed in the tube at points that were 0.25, 0.5, and 0.75 in. from the end.

After the stress gages and ionization pins were emplaced, the tubes were sent to EAFB, where the propellant was cast into them. Our original plan was to use propellant containing approximately 50% HMX. However, because of the propellant classification regulations in force at the time, the propellant we obtained contained approximately 12% HMX. A number of 1-in.-long sections of Lucite tube of the same diameter as the propellant tube were also sent to EAFB. These 1-in. sections, termed add-on sections, were filled with either solid or powdered propellant.

*Kapton is a registered trademark of Du Pont for polyimide film.

†Twinak is a two-conductor-shielded coaxial cable manufactured by Trompeter Electronics.

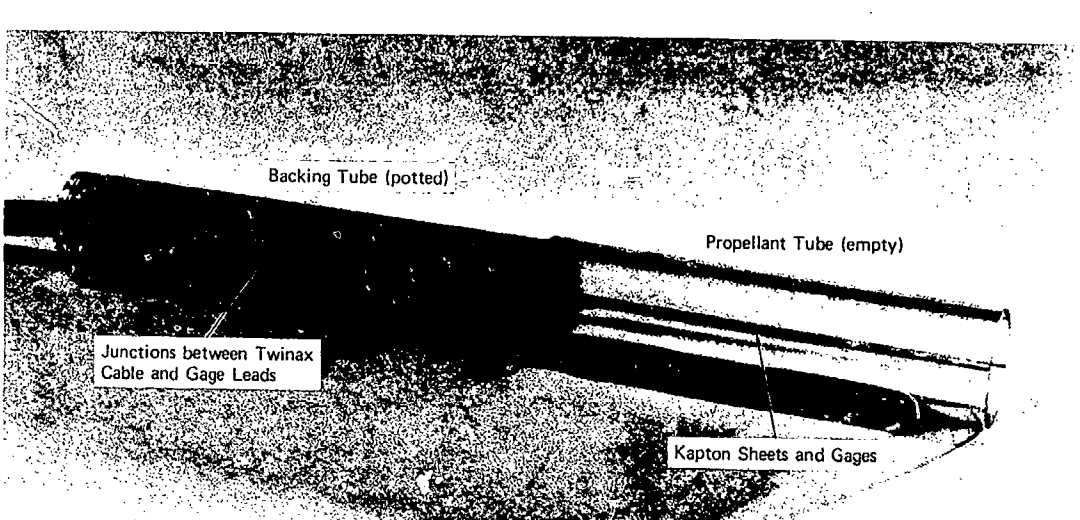

(a) Side View of Kapton Gage Package

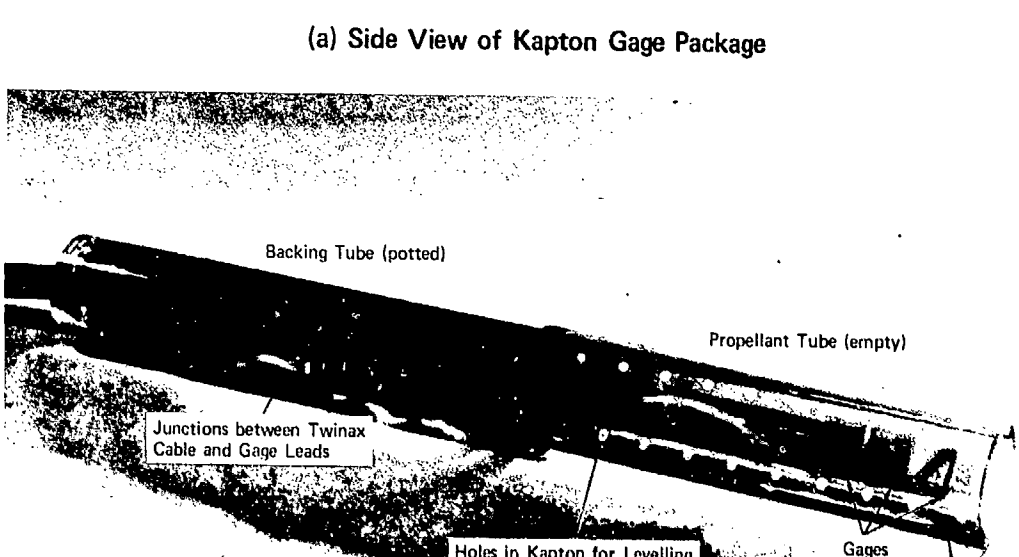

(b) Front View of Kapton Gage Package

MP-6069-11

FIGURE 2 PROPELLANT/BACKING TUBE ASSEMBLY PRIOR TO PROPELLANT CASTING

The powdered propellant supplied for the experiments exhibited a rate of pressure rise of 2.5×10^6 psi/sec in a quickness test performed by personnel at EAFB. Each of the 1-in. add-on sections contained four ionization pins. The pins, 0.25-in. apart, were used to measure the burning rate in the propellant. The purpose of the add-on sections is described in the next section.

4. Experimental Arrangement

Two 1-in.-long add-on sections were added in front of the 10-in. main section of solid propellant in each experiment. We used various combinations of powdered and solid filled add-on sections to vary the burning rate in the propellant. Three experiments were conducted; Table 2 gives the arrangement of the propellant add-on sections. The 10-in. main section, in which the stress gages were emplaced, was used in all experiments.

The add-on sections were taped to the 10-in. solid-propellant section, and a light pipe was epoxied to the outside of the combined cylinder, flush with the igniter end of the propellant tube. The entire propellant tube--containing stress gages, ionization pins, and light pipe--was then placed inside the steel DDT tube so as to butt against the igniter (see Fig. 1). After alignment, the cavity between the propellant tube and the inside diameter of the steel DDT cylinder was filled with epoxy. We used stycast low viscosity Resin No. 3020 with catalyst No. 9.* Because this epoxy has a low exotherm temperautre ($\sim$30°C) it was safe to use with the propellant. A dummy igniter was used to hold the components in the proper positions during the epoxy pour. After the epoxy had hardened, the dummy igniter was removed and the real igniter was inserted and the end caps bolted together. The bolts, 1.25 in. in diameter, were torqued to 1,000 ft-lb each. The leads for the stress gages and ionization pins exited through the end cap opposite the igniter as shown in Fig. 1. The space around the leads was filled with epoxy.

*From Emerson and Cummings, Inc., Gardena, CA 90248.

Table 2

ARRANGEMENT OF PROPELLANT SECTIONS
IN STEEL CONFINEMENT

Propellant Section	Experiment Number		
	1	2	3
First Add-On Section	Solid[a]	Powdered[b]	Powdered[b]
Second Add-On Section	Powdered[b]	Powdered[b]	Solid[a]

[a] Density = 1.95 g/cm^3.

[b] Density = 1.51 g/cm^3.

5. Instrumentation

The signals from the stress gages and ionization pins were recorded on oscilloscopes. The signal from the light pipe, produced when the burning in the igniter mixture reached the igniter-propellant interface, was used to trigger the oscilloscopes; the oscilloscopes recorded the stress gage signals. The power supplies for the stress gages were turned on by the "gate out" from the oscilloscopes recording the stress gage signals. The oscilloscopes that recorded the ionization pins were internally triggered by the signal coming from the first pin that closed. One oscilloscope, triggered by the signal from the light pipe, recorded the signal from the pins. This record was used to time-correlate the stress gages and the ionization pins.

6. Results and Interpretation of Experiments in Steel Tubes

Table 2 shows the arrangement of cracked and solid propellant in the three experiments that were performed in steel tubes. The results of each experiment will be discussed and then some general conclusions will be given.

In the first experiment, in which we had expected stresses in the order of 40 kbar, the stress gages recorded stresses of only about 5 to 7 kbar. Such low stresses indicate that the burning did not produce high-order detonation. Because the instrumentation was set for the expected high stresses, the stress gage records obtained were not optimum quality. No pin records were obtained from this experiment.

Examination of the recovered hardware indicates that at some point during the experiment, venting occurred between the steel DDT cylinder and the end cap at the igniter end. The hardware was recovered still completely assembled, but the bolts had stretched under the internal pressure generated by the burning igniter and propellant. After the experiment, there was a 0.125-in. gap between the igniter end cap and the DDT cylinder. Markings on the hardware indicate that the igniter cup was forced backward and that the hot gases escaped between the

igniter cup and the DDT cylinder. These escaping gases eroded the surfaces of the cup and the inside of the DDT cylinder. Figure 3 shows the loose fit between the igniter cup and the steel cylinder; the preshot tolerance of this fit was 0.003 in. Figures 4(a) and (b) show that the hot escaping gases also eroded the end cap and the bolts.

Although stronger bolts were used in the second and third experiments, venting still occurred and the recovered hardware looked the same as that in the first experiment. The hot escaping gases eroded parts of the end cap, the bolts, and the igniter cup. Interestingly, we recovered pieces of Lucite from inside the confinement cylinder that did not look as if they had been melted.

Stress gage records were obtained from all gages in the second and third experiments. Figure 5 shows the oscilloscope records from Experiment No. 3 and Fig. 6 shows the corresponding reduced stress-time profiles. The data in Fig. 5 and 6 indicate a steady state of stress at each gage position about 100 to 200 μsec after the initial rise. The steady state of stress decreases from gages 1 to 3, however, indicating that the propellant maintains a stress gradient. Gage 3 from experiment 3 recorded for the longest time--about 900 μsec.

The stress waves arrive at the gages much sooner than the flame front. In the first experiment, the stress waves arrived at gage 3 (the best record) about 480 μsec after the flame reached the igniter-propellant interface. In the second and third experiments, the stress waves arrived at the gages just when the flame reached the igniter-propellant interface. Two reasons for this difference are suggested. In the first experiment, weaker bolts were used and the venting may have occurred early, causing a slower pressure buildup. Also, in the first experiment the first propellant add-on section after the igniter was solid propellant, whereas in the second and third experiments the first add-on propellant section was powdered propellant. Thus, the gas generated by the igniter might have entered the propellant more readily in the latter two experiments, resulting in the earlier generation of stress waves.

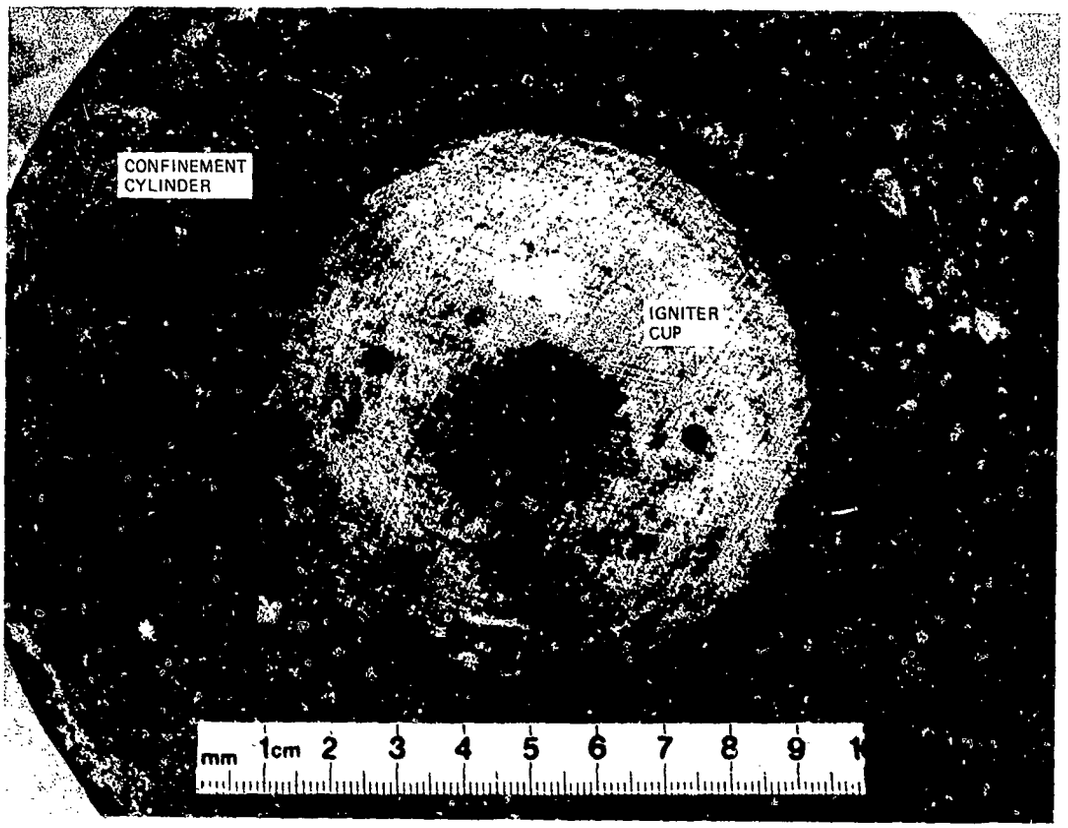

MP-6069-2

FIGURE 3 POST-SHOT PICTURE SHOWING LOOSE FIT BETWEEN IGNITER CUP AND STEEL CONFINEMENT CYLINDER

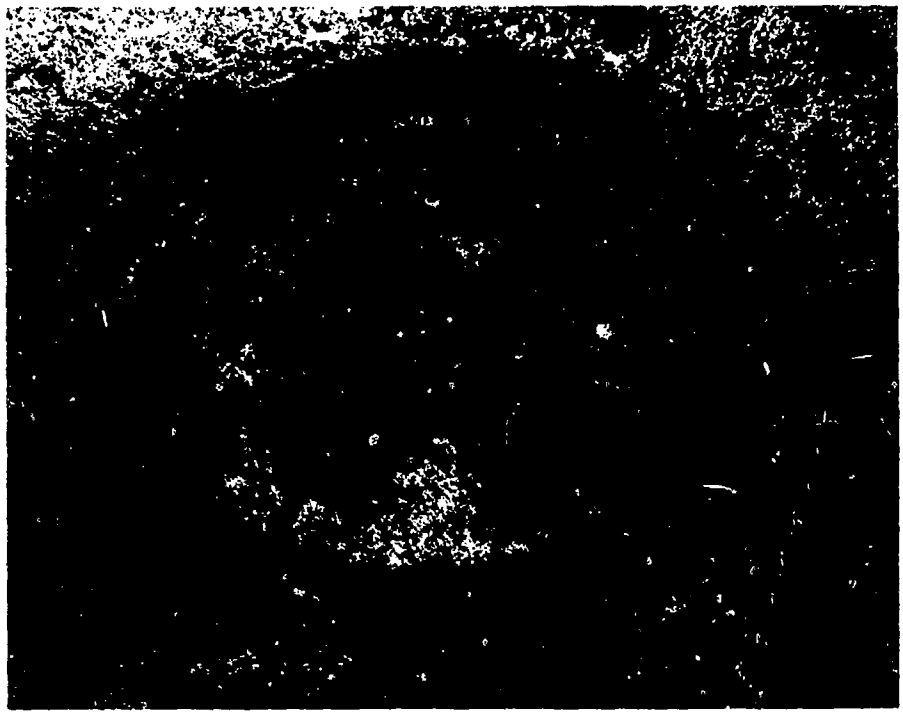

(a) END CAP

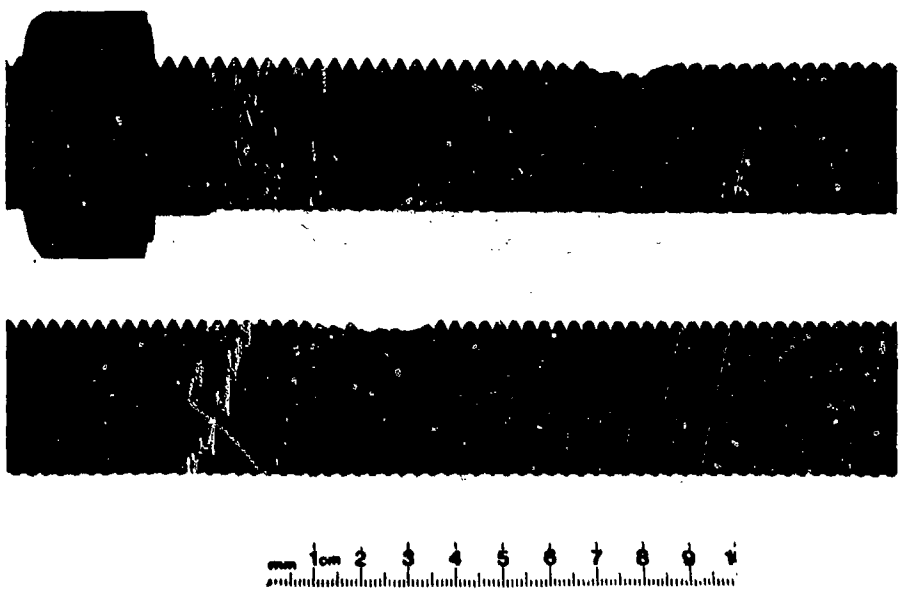

(b) HIGH STRENGTH BOLTS

MP-6069-3

FIGURE 4 POST-SHOT PICTURES SHOWING EROSION OF END CAP AND BOLTS BY HOT ESCAPING GASES

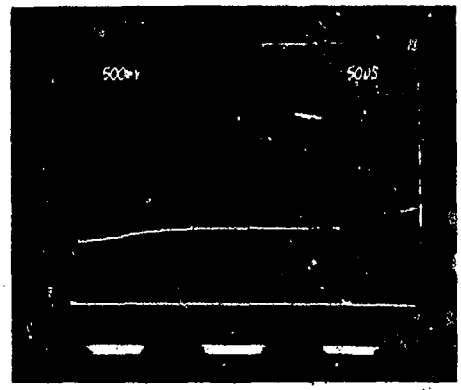

(a) GAGE 1

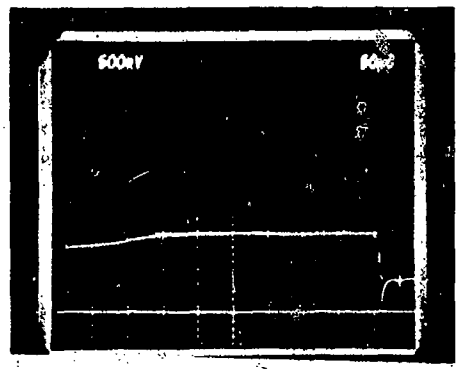

(b) GAGE 2

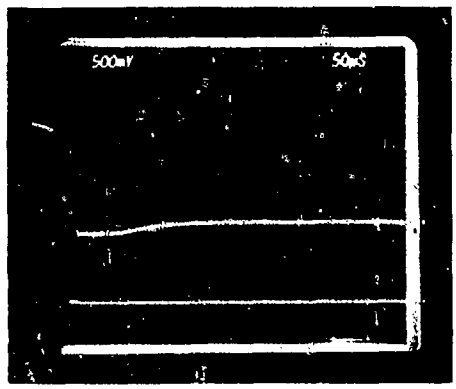

(c) GAGE 3

MP-6069-4

FIGURE 5 OSCILLOSCOPE RECORDS FROM STRESS GAGES IN EXPERIMENT 3

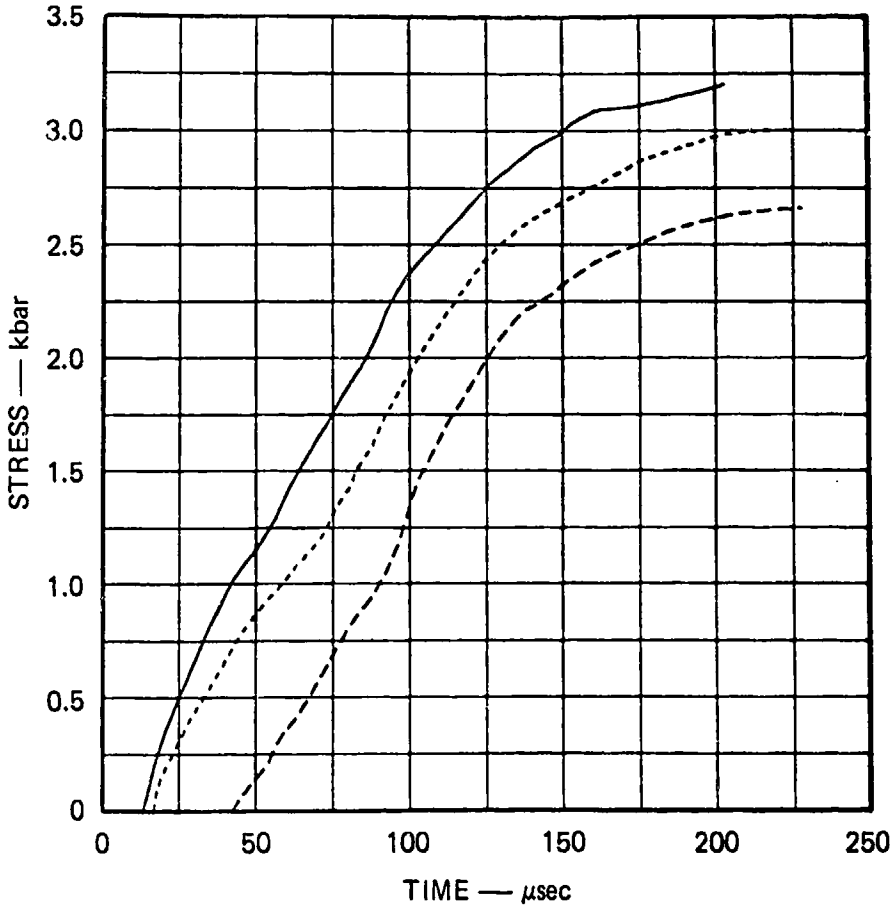

FIGURE 6 STRESS HISTORIES IN PROPELLANT OBTAINED FROM GAGE RECORDS OF EXPERIMENT 3 AND USED FOR LAGRANGE ANALYSIS

Good quality ionization pin records were obtained for experiment No. 3. Seven pin signals were recorded; the results are shown on a distance-time plot in Fig. 7. There is a decided change in slope in the pin results at about 900 μsec. The burning rate determined from the pin data (ignoring the first pin) up to that point was 0.068 mm/μsec. After about 900 μsec, the burning rate slowed to about 0.021 mm/μsec.

7. Lagrange Analysis

The Lagrange stress histories based on experimental data, shown in Fig. 6, were used in a Lagrange analysis to calculate Lagrange particle velocity histories, Lagrange stress-particle velocity paths, and Lagrange stress-specific volume paths in compressed propellant ahead of the flame front. In this Lagrange analysis, the momentum equation [equation (30)] is integrated with the stress gradient that is estimated from the stress records to generate the particle velocity histories at the gage positions. The continuity equation [equation (29)] is then integrated with the particle velocity gradient that is estimated from the particle velocity histories to generate the specific volume histories at the gage positions. The elimination of time between the stress histories and the particle velocity histories gives the corresponding Lagrange stress-specific volume paths. The (u,t) profiles calculated from the (σ,t) records are shown in Fig. 8, and the corresponding Lagrange (σ,u) paths and Lagrange (σ,v) paths are shown in Figs. 9 and 10.

Examination of these profiles shows that the flame produces a compression wave ahead of itself as it propagates along the tube. The stress at a given gage position builds up to a constant value and a constant Lagrange pressure gradient is formed in the compression ahead of the flame. A shock is not formed in front of the flame because, as shown in Figs. 9 and 10, the propellant satisfies the conditions $(\partial^2\sigma/\partial u^2)_h < 0$ and $(\partial^2\sigma/\partial v^2)_h < 0$ in the pressure range produced by the flame. The limited buildup in pressure is attributed to the relatively small amount of HMX in the propellant. Shock formation is expected at higher pressures in this propellant, however, because these second derivatives become positive as the pressure increases.

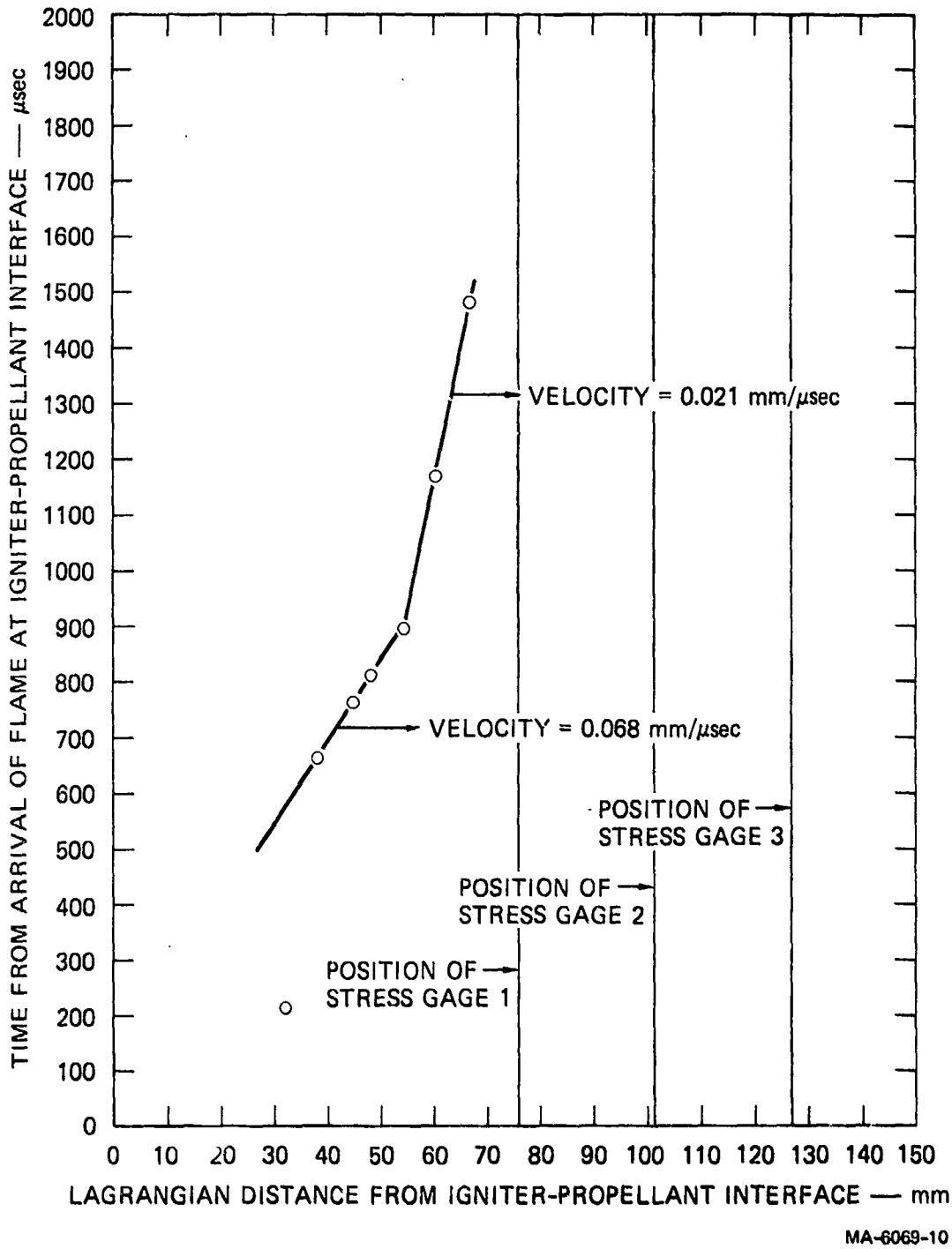

FIGURE 7 IONIZATION PIN DATA

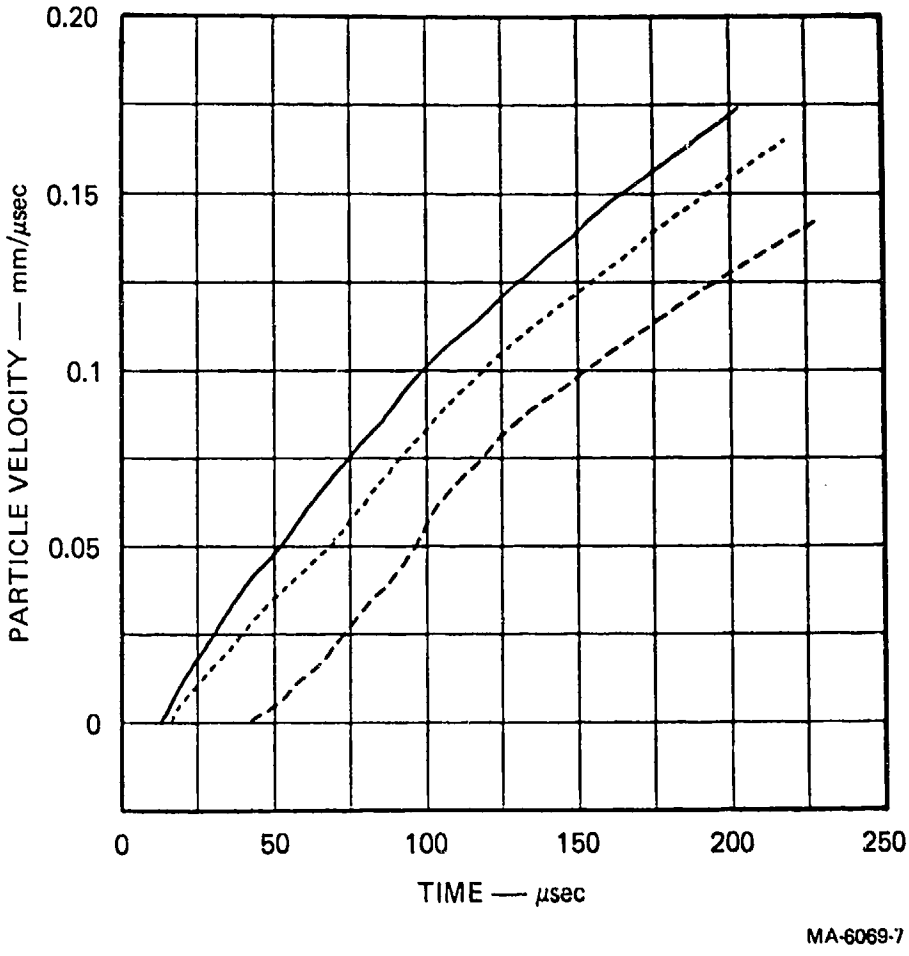

FIGURE 8 PARTICLE VELOCITY HISTORIES CALCULATED FROM THE STRESS HISTORIES SHOWN IN FIGURE 6

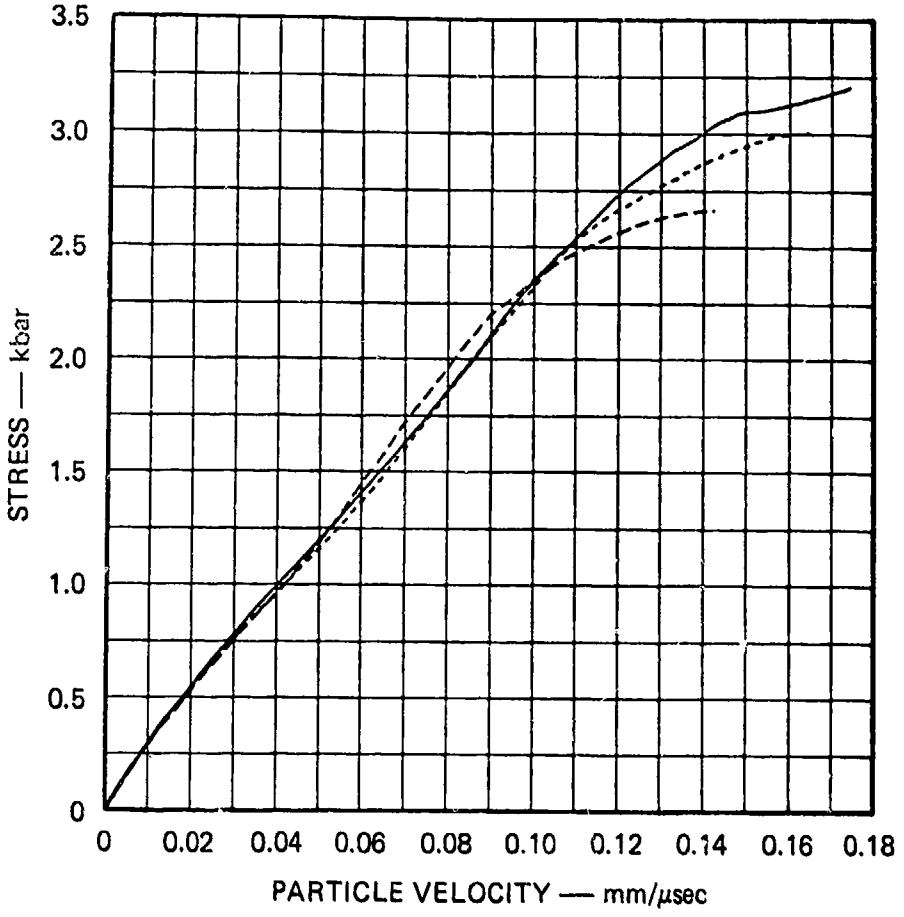

FIGURE 9 LAGRANGE STRESS-PARTICLE VELOCITY PATHS CALCULATED FROM THE STRESS HISTORIES SHOWN IN FIGURE 6

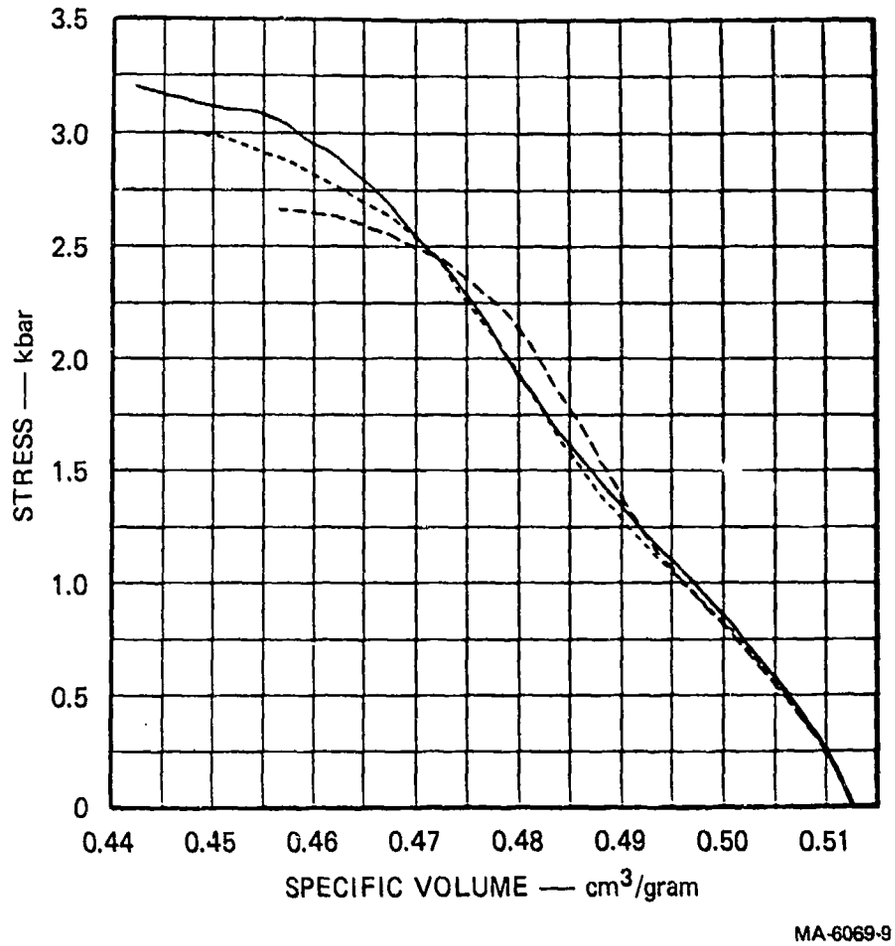

FIGURE 10 LAGRANGE STRESS-VOLUME PATHS CALCULATED FROM THE STRESS HISTORIES SHOWN IN FIGURE 6

B. Experiments in Lexan Tubes

The propellant KW-6 used in these experiments contained 50% HMX. The confinement was changed from steel to Lexan for this propellant with the higher percentage of HMX to make the experimental configuration much lighter and more manageable. The experimental arrangement is shown schematically in Fig. 11. It consisted of a thick-walled confinement tube of Lexan polycarbonate, a PMMA tube containing ionization pins and propellant, an igniter cup, aluminum end plugs, steel end plates, and bolts and nuts of clamp the end caps and plates tightly to the confinement tube.

1. DDT Confinement Tube

The confinement tube was made of Lexan, a polycarbonate. It was 18-in. long with an outside diameter of 6 in. and an inside diameter of 3 in. The confinement tube, end plugs, end plates, and clamping bolts were designed to confine the high gas pressures, generated by the igniter and by the burning propellant, until pressures of the order of thousands of bars were reached. The inside diameter of the tube was large enough to make any diameter effect on burning negligible and large enough to exceed the critical diameter of the propellant.

Two Viton* o-rings were placed over the confinement tube at the igniter end to form a temporary gas-tight seal between the confinement tube and the aluminum end cap (see Fig. 11). The high temperature performance of the Viton o-rings would seal against the hot gases for the life-time of the experiment (several seconds). Double o-rings were used to extend the lifetime of the seal.

The end cap and steel plate of the igniter end had holes through which the igniter leads and light pipe passed. At the opposite end, the end cap and steel plate had exit holes for the ionization pin leads and the stress gage leads.

*Viton - Trade name for Fluorelastomer manufactured by E. I. duPont de Nemours and Co. Inc.

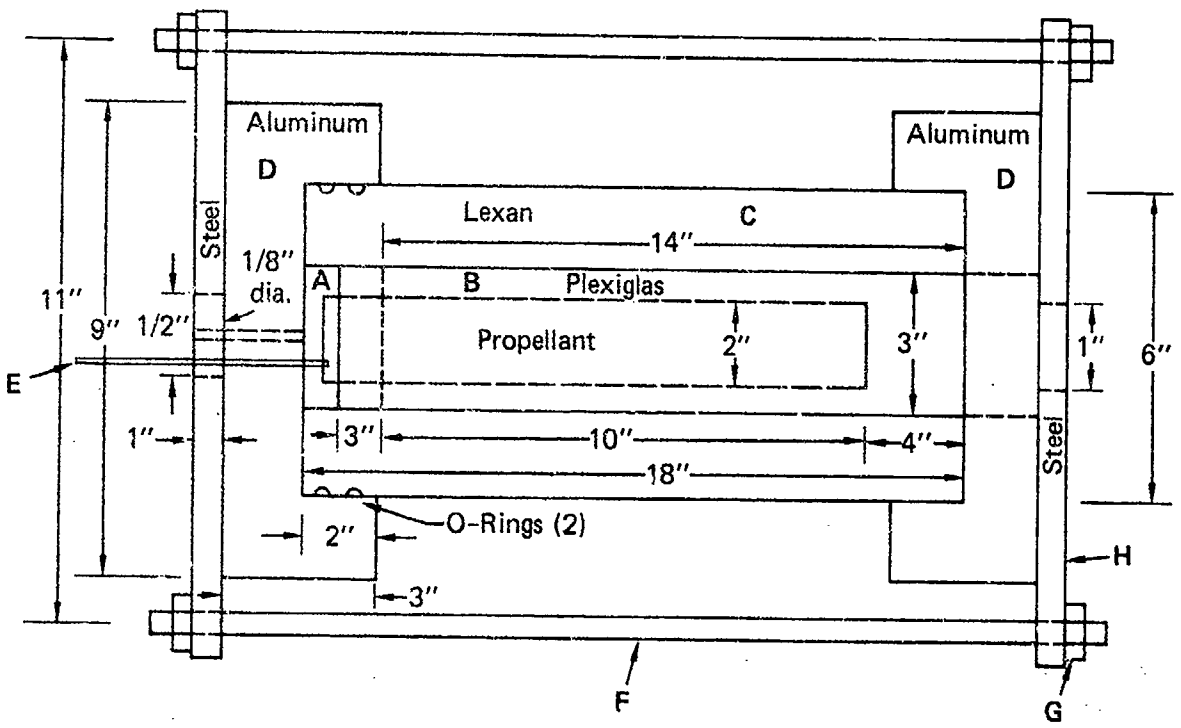

FIGURE 11 SCHEMATIC DRAWING OF EXPERIMENTAL ARRANGEMENT IN LEXAN CONFINEMENT

A = Igniter Cup Assembly
B = PMMA Tube Containing Propellant
C = Lexan DDT Confinement Tube
D = End Caps
E = Light Pipe
F = High Strength Bolts
G = Nuts
H = Steel End Plates

2. Igniter

The igniter material was a mixture of boron and potassium nitrate with a laminac-lubersol binder obtained from Polytechnic Specialities in Byron, Georgia. The mixture was 22.7% boron, 71.7% potassium nitrate, and 5.6% binder. This mixture generates about 1600 cal/g of material. Approximately 16 g of the igniter powder was placed in a Lucite cup lined on the bottom with nichrome heating ribbon. The cup had an inside diameter of 2 in. and a depth of 0.5 in. The Lucite cup was placed in a steel cup which fit inside the Lexan confinement tube as shown in Fig. 11.

The nichrome heater ribbon was about 11-in. long, 0.06-in. wide, and 0.007-in. thick, with a resistance of about 1 ohm. The igniter leads were brought out the rear of the igniter assembly through the aluminum end plugs and steel end plates. The igniter material was thermally initiated using a 28-volt, 5-amp dc power supply to heat the nichrome ribbon.

3. Propellant Tube and Propellant

The PMMA tube used to contain the propellant inside the Lexan confinement tube is shown in Fig. 12. This tube was to serve as a casting mold for the propellant and a jig for holding the ytterbium stress gages during casting. The main section of this tube was 2-in. long and the outside diameter was 3 in. This section was slit lengthwise down the center of the cylinder to support the gages.

Four ytterbium stress gages were glued to a sheet of Kapton,* their leads were insulated from one another by additional layers of Kapton. The resulting Kapton sheet with gages was then glued between the two PMMA half cylinders, as shown in Fig. 12(a). The stress gages were located 1, 3, 5, and 7 in. from the end of the cylinder. The gage leads were attached to Twinax+ coaxial cable and potted with epoxy inside the last 4 in. of the PMMA tube. The backing tube was to delay the arrival at the gages of stress waves reflected from the end of the tube.

*Kapton is a registered trademark of DuPont for polyimide film.

+Twinax is a two-conductor shielded coaxial cable manufactured by Trompter Electronics.

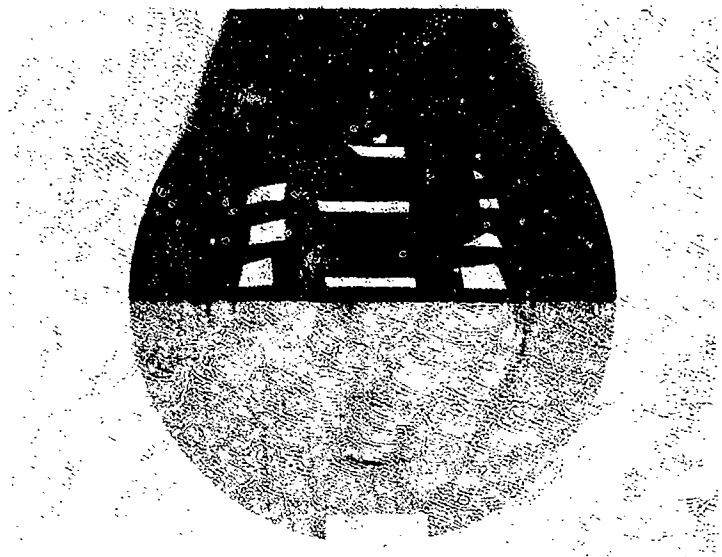

(a) END VIEW SHOWING STRESS GAGES AND GROOVES FOR IONIZATION PIN LEADS

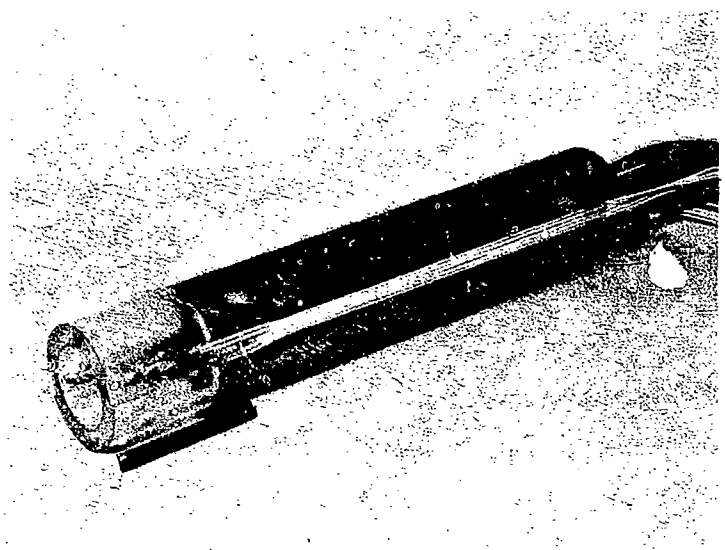

(b) SIDE VIEW SHOWING IONIZATION PIN SECTION IN PLACE AND LEADS IN GROOVES

MP-6069-19

FIGURE 12 PMMA TUBE CONTAINING PROPELLANT AND YTTERBIUM STRESS GAGES

The ytterbium gages were cut from 0.002-in.-thick ytterbium foil. Each gage was 0.6-in. long with four legs (see Fig. 12(b)). The two outside legs of each gage were connected to the gage power supply. The gage voltage was measured across the two inside legs. The resistance of each gage was approximately 0.25 Ω.

A 3-in.-long PMMA section was placed in front of the gage section of the tube. This short tube section containing ionization pins is shown in place in Fig. 12(b). A groove was cut in either side of the PMMA propellant tube and short tube in which the ionization pin leads were placed as shown in Fig. 12(b). By placing the leads in grooves, the whole assembly could be inserted into the confinement tube.

Ionization pins were placed on either side of the short section so that the pins were 1/4-in. apart as shown in Figure 13. The pins were cemented in place in steel collars with Eastman 910. The lead ends of the pins were bent flush along the bottom of the grooves and the leads were epoxied in the grooves along the sides of the short tube and the propellant tube as shown in Fig. 12(b) and Fig. 13.

After the stress gages and ionization pins were emplaced, the tubes were sent to EAFB, where the propellant was cast into them. The propellant KW-6 contained 50% HMX.

4. Experimental Arrangement

The tubes filled with propellant were sent to us by Lt. Steven Cliff of EAFB. The propellant was cast into three of the long PMMA tubes and two of the short PMMA tubes. The density was 2.27 g/cm^3. The other tubes of each kind were filled with powdered propellant packed to a density of 65% of the cast density. By using combinations of powdered and cast propellant, we hoped to control the burning rate in the propellant and observe the effect on stress wave propagation and buildup at the ytterbium gage positions. Five experiments were conducted with the combinations shown in Table 3.

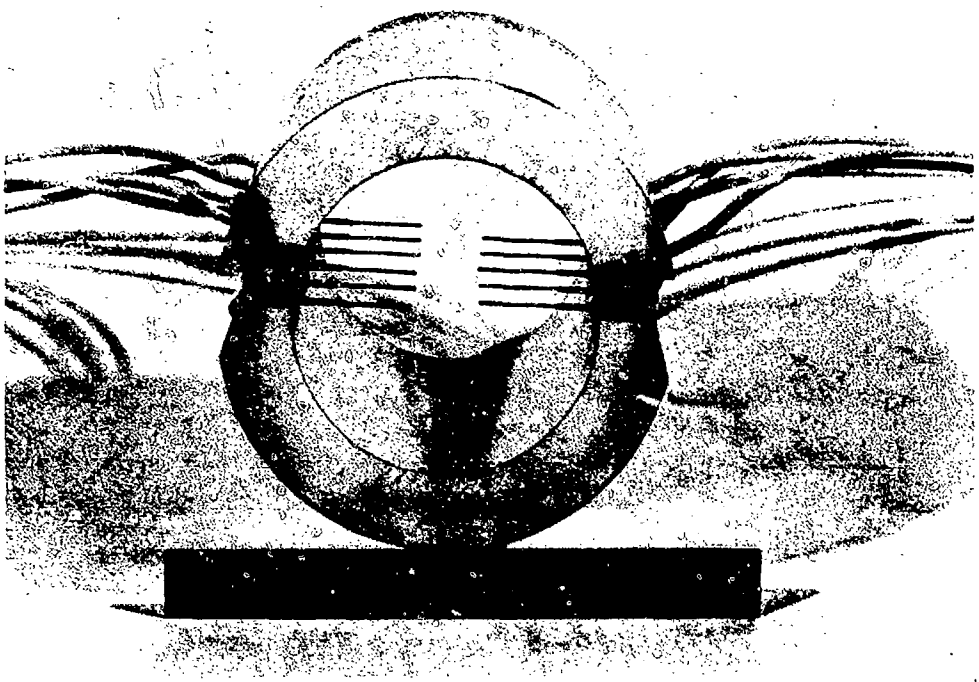

MP-6069-20

FIGURE 13 IONIZATION PIN SECTION SHOWING PINS IN PLACE

Table 3

ARRANGEMENT OF PROPELLANT SECTIONS IN LEXAN CONFINEMENT

	Experiment Number				
Propellant Section	1	2	3	4	5
Short-Pin Section	Cast	Powdered	Powdered	Cast	Powdered
Long-Gage Section	Cast	Powdered	Powdered	Cast	Cast

The short sections containing the ionization pins were placed at the appropriate end of the long section containing the ytterbium gages, and the pin leads were dressed in the grooves along the side of the long tubes as shown in Fig. 12(b). This assembly was inserted into the Lexan confinement tube. The igniter assembly was fitted in place, the o-rings placed on the confinement tube, and the end plugs and steel end plates put in place and bolted together. Figure 14(a) shows the components arranged for assembly and Fig. 14(b) shows them assembled with 2 of 6 bolts installed. The bolts were 3/4-in. diameter and were torqued to 500 ft-lb each.

5. Instrumentation

The signals from the stress gages and ionization pins were recorded on oscilloscopes and also on a 500- kilohertz Fm tape recorder. The signal from the light pipe, produced by the burning igniter mixture, triggered the electronics. The oscilloscopes recording the ionization pins were triggered promptly while the oscilloscopes recording the stress gage signals were triggered through appropriate delays. The power supplies for the stress gages were turned on by the "gate out" from the oscilloscopes recording the stress gage signals.

The tape recorder has essentially an "infinite" time coverage, so it was triggered promptly by the signal from the light pipe. The ionization pins were coded and recorded on two separate channels. Each stress gage was recorded on a separate channel, The results from the tape recorder were used to time-correlate the stress gages and ionization pins.

6. Results and Interpretation of Experiments in Lexan Tubes.

Table 3 shows the arrangement of cast and powdered propellant in the five experiments that were performed. Pin records were obtained in all of these experiments but ytterbium gage records were obtained in only the first three. The pin records were used to calculate burning rates. The gage records were used as input in a Lagrange analysis to

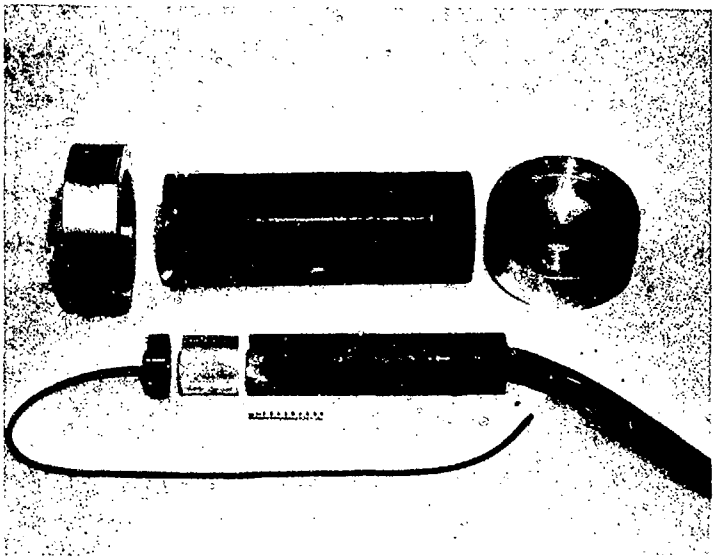

(a) HARDWARE BEFORE ASSEMBLY

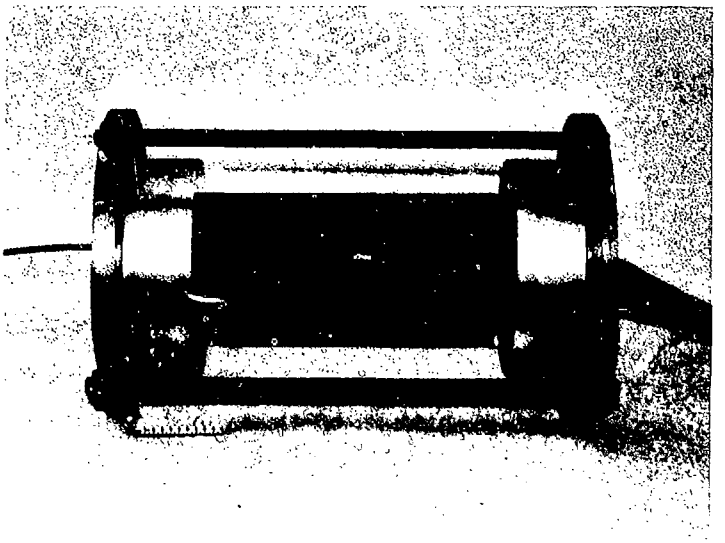

(b) ASSEMBLED EXPERIMENT

MP-6069-21

FIGURE 14 COMPONENTS OF DDT EXPERIMENT

integrate the equations of motion, equations (29) and (30) and determine the states produced in front of the flame. Values of the particle velocity and specific volume calculated from the gage records in the Lagrange analysis were, however, found to be unrealistic. The calculated particle velocities were much too high and the calculated specific volumes were much too low. These unrealistic values were obtained because consecutive gage records are separated by times about a factor of 5 greater than those expected in a one-dimensional compression or rarefaction wave. Because the gage histories measured by the oscilloscopes and the tape recorder agree, and no such problem was encountered in the DDT experiments performed in steel tubes, we conclude that the Lexan tube did not provide one-dimensional confinement to the propellant in front of the flame. For this reason, we only present here the burn velocities, the maximum stresses calculated from the gage records, and the velocities between gages in uncompressed propellant calculated from the gage records. These data are given in Table 4.

Examination of the Lexan tubes after the completion of the experiments led to the conclusion that while DDT did not occur in experiments 1, 3, 4, and 5, it may have occurred in experiment 2 with the highest calculated pressure. Although the burning rate was higher in experiment 3 than in experiment 2, venting occurred in experiment 3 at the end of the tube housing the gage-leads.

We conclude that Lexan does not provide the confinement required for a successful Lagrange gage study of DDT, and we recommend the use of steel-confining tubes in any such study that may be undertaken in the future.

Table 4

EXPERIMENTAL RESULTS FOR LEXAN CONFINEMENT

	Burn Velocity (mm/μs)	Maximum Pressure (kbar)	Wave Velocity* (mm/μs)
	0.066		
Experiment 1	0.045	1.9	0.5
Experiment 2	0.12	>35	0.22
Experiment 3	0.18	4+	0.24
Experiment 4	0.07	-[a]	-
Experiment 5	0.06	-[a]	-

*From arrival lines.

+Gage Stretched.

[a]No gage records were obtained.

REFERENCES

1. R. Courant and K. O. Friendricks, Supersonic Flows and Shock Waves (Interscience, New York, New York, 1948).

2. M. Cowperthwaite and R. F. Williams, "Determination of Constitutive Relations with Multiple Gages in Nondivergent Waves," J. Appl. Phys, 42, p. 456 (1971).

3. H. Jones, "Accelerated Flames and Detonation in Gages," Proc. Roy. Soc. A248, No. 1254, p. 333 (1958).

4. G. K. Adams and D. C. Pack, "Some Observations on the Problem of Transition Between Deflagration and Detonation," Seventh Symposium (International) on Combustion, P. 812 (Butterworths, London, 1959).

5. A. Macek, "Transition from Deflagration to Detonation in Cast Explosive," J. Chem. Phys. 31, p. 162 (1959).

6. C. M. Tarver, T. C. Goodale, R. Shaw, and M. Cowperthwaite, "Deflagration-to-Detonation Transition Studies for Two Potential Isomine Cast Primary Explosives," Proceedings of the Sixth Symposium (International) on Detonation, ACR-221, p. 231, Office of Naval Research (1976).

7. I. D. Landau and E. M. Lifshitz, Fluid Mechanics, p. 374 (Pergamon Press London, Paris, Frankfurt, 1959, Addison-Wesley Publishing Company Inc., Reading, Massachusetts).

Appendix

PHENOMENOLOGY OF THE DEFLAGRATION TO DETONATION TRANSITION IN PROPELLANTS AND EXPLOSIVES

PHENOMENOLOGY OF THE DEFLAGRATION TO DETONATION TRANSITION IN PROPELLANTS AND EXPLOSIVES*

M. Cowperthwaite
SRI International
Menlo Park, CA 94025

Model solutions are presented for the deflagration to shock transition (DST) process associated with the propagation of an accelerating flame in propellant contained in a closed tube. The flame is treated as a reactive discontinuity, the flow in front of the flame as a simple compression wave, and the density gradient in the flow behind the flame is assumed to be zero. The solutions are based on expressions for the burning rate and the acceleration of the flame and are valid until the time the reaction becomes complete in the flame. Consideration of the evolution of the shock preceding the flame after this time led to a postulate for assessing the probable occurrence of the deflagration to detonation transition (DDT). Examination of particular solutions in the light of this postulate showed that DDT depends strongly on the burning rate and will probably not occur unless the burning rate parameter exceeds a critical value.

INTRODUCTION

The deflagration to detonation transition (DDT) in a propellant or explosive is said to occur when the propagation of a flame results in the formation of a detonation wave in front of the flame. Significant events envisaged in the evolution of DDT are as follows:

- The formation of an accelerating flame by an unsteady burning process.
- The formation of a shock wave in unburnt material by the compressive action of the accelerating flame in the deflagration to shock transition (DST).
- The formation of a detonation wave in material ahead of the flame by the shock to detonation transition (SDT).

We are concerned in the present paper with the occurrence of DDT in a burning propellant contained in a closed tube. Our approach to this problem is based on the premise that it is valid to model DDT by the above chain of events when the burning process is subject to the confinement provided by a closed tube. In this case, DDT will not occur unless the accelerating flame produces a shock wave and the properties of this shock satisfy the conditions required for the occurrence of SDT. The condition for shock formation is thus not a criticality condition for DDT, and the shock must be characterized to assess the probability of the occurrence of DDT. It is for this reason that our present phenomenological treatment of DDT is restricted primarily to an analytic treatment of DST.

TREATMENT OF DDT

Our approach is based on the premise that the dynamics of the flow behind and in front of an accelerating flame must be considered to characterize the shock formed in front of the flame and assess the probability of DDT. In this case, an analytical treatment of DDT must model the accelerating flame, and the unsteady flows on both sides of it. The model for these unsteady processes used in the present paper is based on the model formulated by Jones [1] to investigate the DDT process in gases. We treat the flame as a reactive discontinuity, the flow in front of the flame as a simple compression wave, and we assume that the density gradient is zero in the flow behind the flame. The one-dimensional differential equations governing this type of flow in a closed tube can be solved when a relationship for the burning rate is known and the acceleration of the flame is prescribed. The validity of such solutions must be questioned as the flow develops however because the equation used to prescribe the

*This work was supported by the Air Force Office of Scientific Research under Contract F49620-77-C-0039.

acceleration of the flame may become incompatible with the Hugoniot equation expressing the balance of energy across the flame. The solution presented here is only valid until the time (t_R) the reaction becomes complete in flame because the Hugoniot equation shows that the extent of reaction increases in the flame as the flow develops. Particular solutions were constructed and examined over the time intervals defined by the reaction times to determine the times taken for shock formation in front of the flame, and the position and strength of these shocks at later times. The strength of the shock when all the chemical energy is liberated in the flame is then used to relate the probability of DDT to the burning rate. Our treatment is phenomenological but supercedes previous thermo-hydrodynamic treatments [2-4] by making the states attained across the flame compatible with the differential equations governing the conservation of mass and momentum in the flow behind the flame as well as with the rear-boundary particle velocity condition in the closed tube.

SOLUTION FOR DST

We let the superscript f and F denote respectively the flame discontinuity and its propagation velocity, and we let the subscripts + and - denote quantities in front of and behind the flame. States across the flame are related by the Rankine-Hugoniot jump conditions written as

$$\rho_+^f(F - u_+^f) = \rho_-^f(F - u_-^f) \tag{1}$$

$$p_+^f - p_-^f = \rho_+^f(F - u_+^f)(u_+^f - u_-^f) \tag{2}$$

$$2(e_-^f - e_+^f) = (p_+^f + p_-^f)(v_+^f - v_-^f) \tag{3}$$

where ρ, u, p, and e denote density, particle velocity, pressure and specific energy, and $v = 1/\rho$ denotes the specific volume. We let c denote the sound speed and the subscript o denote the initial state in the propellant, and we assume that the propellant is governed by a Murnaghan equation with an index n = 3. The equations for p_+, ρ_+, e_+, and the slope of a forward facing C_+ characteristics ($u_+ + c_+$) in the simple isentropic compression wave can then be written as

$$p_+ = \frac{c_o^2\rho_o}{3}\left[\left(1 + \frac{u_+}{c_o}\right)^3 - 1\right] + p_o \tag{4}$$

$$\rho_+ = \rho_o\left(1 + \frac{u_+}{c_o}\right) \tag{5}$$

$$e_+ = e_o + \frac{(p_+ - p_o)v_+}{2} + \frac{(\rho_o c_o^2 - 2p_o)}{2}(v_+ - v_o) \tag{6}$$

$$u_+ + c_+ = c_o + 2u_+ \tag{7}$$

We denote the extent and heat of reaction by λ and q, assume that the reaction products are polytropic with an index k = 3, and write the equation of state for material behind the flame as

$$e_- = e_o - \lambda q + \frac{(pv)_-}{2} - \frac{\lambda p_o v_o^p}{2} - (1 - \lambda)\frac{p_o v_+(p_-)}{2} + (1 - \lambda)\frac{(c_o^2\rho_o - 2p_o)}{2}(v_+(p_-) - v_o) \tag{8}$$

where $v_+(p_-)$ is written to denote that the volume of the propellant is related to the pressure by the same equation on both sides of the flame and v_o^p denotes the specific volume of the detonation products in their standard state. The combination of Eqs. (3), (6), and (8) allows us to write the extent of reaction in the flame as

$$\lambda^f = \Delta E^f/Q^f \tag{9}$$

where $Q^f = [2q + p_o(v_o^p - v_o) + (c_o^2\rho_o - 3p_o) \times (v_+(p_-^f) - v_o)]$ 9a

and $\Delta E^f = [(p_- + p_+)(v_- - v_+) + (pv)_- - (pv)_+ + (c_o^2\rho_o - 3p_o)(v_+(p_-) - v_o)]^f$ 9b

with f written as a superscript on the bracket for notational convenience.

We let x and t denote Eulerian distance and time so that $F = dx^f/dt$. In contrast to Jones [1], we assume that the burning rate is related to the particle velocity and the pressure at the flame front by the equation

$$F = u_+^f + A(p_+^f - p_o) \tag{10}$$

where A is a parameter. The assumption that the pressure exponent in Eq. (10) is 1 is not necessary but is made here for convenience.

We prescribe the acceleration of the flame by the assumption that the particle velocity at the flame front is governed by a power law of the form

$$u_+^f = \alpha_m t^m \tag{11}$$

with α_m and m considered as parameters.

We are now in a position to construct the solution for the flow produced by our accelerating flame. We write the differential equations for the flow in front of the flame as

$$\frac{\partial\rho_+}{\partial t} + u_+\frac{\partial\rho_+}{\partial x} + \rho_+\frac{\partial u_+}{\partial x} = 0 \tag{12}$$

$$\frac{\partial u_+}{\partial t} + u_+ \frac{\partial u_+}{\partial x} + \rho_+^{-1}\left(\frac{dp}{d\rho}\right)_+ \frac{\partial p_+}{\partial x} = 0 \qquad (13)$$

to satisfy the isentropic condition, and we write the differential equation for the flow behind the flame as

$$\frac{\partial \rho_-}{\partial t} + \rho_- \frac{\partial u_-}{\partial x} = 0 \qquad (14)$$

$$\frac{\partial u_-}{\partial t} + u_- \frac{\partial u_-}{\partial x} + \rho_-^{-1} \frac{\partial p_-}{\partial x} = 0 \qquad (15)$$

to satisfy the assumption that $\partial\rho_-/\partial x = 0$ behind the flame. It is convenient to construct the solution in terms of u_+^f rather than t. The procedure is as follows: (1) calculate the flame trajectory, (2) calculate the time for shock formation t_s in front of the flame, and (3) calculate the density behind the flame to determine the burnt state, the $u_-(x,t)$ and $p_-(x,t)$ fields behind the flame, and the reaction time t_R.

We will now carry out these steps in detail:

(1) Calculation of the Flame Trajectory

We first combine Eqs. (4) and (10) to derive the following equation for the flame speed in terms of u_+^f,

$$F = B\left[\left(3 + \frac{c_o}{B}\right)\frac{u_+^f}{c_o} + 3\left(\frac{u_+^f}{c_o}\right)^2 + \left(\frac{u_+^f}{c_o}\right)^3\right] \qquad (16)$$

where $B = A c_o^2 \rho_o/3$. The exponent of the pressure in Eq. (10) was assumed to be 1 in order to obtain this simple expression for F. We combine Eq. (16) with the identity

$$\left(\frac{dx}{du_+}\right)^f = F \frac{dt}{du_+^f} \qquad (17)$$

to obtain a differential equation for x^f and integrate it with

$$\frac{dt}{du_+^f} = C\left(\frac{u_+^f}{c_o}\right)^{\frac{1-m}{m}} \qquad (18)$$

and $mC = (\alpha_m)^{-1/m}(c_o)^{(1-m)/m}$ derived from Eq. (11) to obtain the following expression for x^f,

$$x^f = mBCc_o\left(\frac{u_+^f}{c_o}\right)^{\frac{1+m}{m}}\left[\frac{(3 + c_o/B)}{1+m} + \frac{3}{1+2m}\left(\frac{u_+^f}{c_o}\right) + \frac{1}{1+3m}\left(\frac{u_+^f}{c_o}\right)^2\right] \qquad (19)$$

The equation for the position of the flame as a function of time is simply obtained by combining Eqs. (19) and (11).

(2) Shock Formation in Front of the Flame

A shock is formed in the compression wave ahead of an accelerating flame when the propellant satisfies the condition $(d^2p/d\rho^2)_+ > 0$ because the C_+ characteristics emanating from the flame front form an envelope. Since the discontinuity occurs in the flow where $\partial x/\partial u_+ = \partial^2 x/\partial u_+^2 = 0$, application of these conditions to the particle velocity field determines the position x_s and the time t_s of its formation. When Eqs. (12) and (13) are integrated by the method of characteristics from the flame front, the particle velocity field in the compression wave can be written as

$$x = (c_o + 2u_+^f)t + f(u_+^f) \qquad (20)$$

with $f(u_+^f) = x^f - (c_o + 2u_+^f)t^f$ and x^f and t^f defined in terms of u_+^f by Eqs. (19) and (11). Formulating the conditions $\partial x/\partial u_+^f = \partial^2 x/\partial(u_+^f)^2 = 0$ with Eqs. (20), (19), and (11) leads after some manipulation to the equations

$$t_s(u_+^f) = t^f - \left(\frac{F(u_+^f) - (c_o + 2u_+^f)}{2}\right)\frac{dt^f}{du_+^f} \qquad (21)$$

$$\left(\frac{2(m+1)u_+^f}{(m-1)} + F(u_+^f) - \frac{mu_+^f}{(m-1)}\frac{dF}{du_+^f} - c_o\right)x \qquad (22)$$

$$\frac{d^2t^f}{d(u_+^f)^2} = 0$$

where

$$\frac{d^2t^f}{d(u_+^f)^2} = \frac{(1-m)}{mu_+^f}\frac{dt^f}{du_+^f} \text{ and } t^f = mu_+^f\frac{dt^f}{du_+^f}.$$

When $m = 1$, and $d^2t^f/d(u_+^f)^2 = 0$ everywhere in the flow, the equation for the envelope of the characteristics written as

$$x = c_o t + x^f + (2u_+^f - F(u_+^f))t^f \qquad (23)$$

shows that the shock is formed on the first characteristic where $t^f = x^f = u_+^f = 0$. Setting $t^f = h_+^f = u_+^f = F(u_+^f) = 0$ in Eq. (21) then gives the time the shock is formed on the first characteristic as

$$t_s(0) = \frac{c_o}{2\alpha_1} \qquad (24)$$

When $m \neq 1$, the condition

$$\frac{2(m+1)u_+^f}{(m-1)} + F(u_+^f) - \frac{mu_+^f}{(m-1)}\frac{dF}{du_+^f} = c_o \qquad (25)$$

must be solved to find the particle velocity $(u_+^f)_s$, and the characteristic associated with the discontinuity. The time the shock is formed t_s can then be calculated from Eq. (21) and the position where it is formed can be calculated from Eq. (20). Attention in this paper is focused on the case when $m = 1$.

The evolution of the shock after t_s is determined by applying a graphical method [5] to the region of the simple wave where the particle velocity becomes double valued. In this graphical method based on a weak shock approximation, the position of the discontinuity in the $(u_+ - x)$ plane is determined by the condition that the areas between the $(u_+ - x)$ profile and the discontinuity are the same on both sides of the discontinuity.

(3) Calculation of States Behind the Flame

The calculation of states behind the flame is based on the assumption that $(\partial\rho_-/\partial x) = 0$. In this case, the density ρ_- can be readily calculated from an equation expressing the conservation of mass. Since $\rho_- = \rho_+^f$, the calculated density can be used to calculate u_-^f and p_-^f from the jump conditions, Eqs. (1) and (2), and these values can be used to complete the characterization of the $u_-(x,t)$ and $p_-(x,t)$ fields behind the flame. The following expression for ρ_-,

$$\rho_- x^f = \int_o^{u_+^f} \rho_+^f (F - u_+^f)\frac{dt}{du_+^f}\, du_+^f \qquad (26)$$

is obtained as an integral expression for the conservation of mass by equating the mass behind the flame with the mass that passed through the flame front. The mass behind the flame can be written simply as $\rho_- x^f$ because ρ_- can be taken outside the integral $\int_o^{x^f} \rho_- dx$ when $(\partial\rho_-/\partial x) = 0$.

When the integration in Eq. (26) is performed, ρ_- can be written in terms of u_+^f as

$$\rho_-(u_+^f) = \rho_o \frac{B\,C\,c_o^m}{x^f(u_+^f)}\left(\frac{u_+^f}{c_o}\right)^{\frac{1+m}{m}}\left[\frac{3}{(1+m)} + \frac{6}{(1+2m)}\left(\frac{u_+^f}{c_o}\right) + \frac{4}{(1+3m)}\left(\frac{u_+^f}{c_o}\right)^2 + \frac{1}{(1+4m)}\left(\frac{u_+^f}{c_o}\right)^3\right] \qquad (27)$$

with $x^f(u_+^f)$ given by Eq. (19). The combination of Eqs. (27) and (19) gives the equation for the density ratio ρ_-/ρ_o in terms of u_+^f. When ρ_-/ρ_o is known, the following equations obtained from Eqs. (1), (2) and (10),

$$u_-^f = u_+^f - A\,p_+^f\left(\frac{\rho_+^f/\rho_o}{\rho_-/\rho_o} - 1\right) \qquad (28)$$

$$p_-^f = p_+^f - \rho_+^f\left(A\,p_+^f\right)^2\left(\frac{\rho_+^f/\rho_o}{\rho_-/\rho_o} - 1\right) \qquad (29)$$

can be used to calculate u_-^f and p_-^f as a function of u_+^f.

The assumption that $\rho_- = \rho_-(t)$ is also used to construct the equations for the particle velocity and pressure behind the flame. It follows from Eq. (14) that the particle velocity gradient behind the flame is only a function of time and can be written as

$$\left(\frac{\partial u_-}{\partial x}\right) = \eta(t) \qquad (30)$$

Integrating Eq. (30) and making use of the boundary condition $u_- = 0$ at $x = 0$ gives the equation for the particle velocity field behind the flame as

$$u_- = \eta(t)x \qquad (31)$$

where $\eta(t) = u_-^f(t)/x^f(t)$ and $0 < x \leq x^f$. Integration of Eq. (15) with the expression for the acceleration derived from Eq. (31) then gives the equation for the pressure field behind the flame as

$$p_- = p_-^f(t) + \frac{\rho_-}{2}\left(\eta^2 + \frac{d\eta}{dt}\right)\left((x^f(t))^2 - x^2\right) \qquad (32)$$

When p_-^f and v_-^f have been calculated as functions of u_+^f, the time t_R for reaction to go to completion in the flame can be calculated from Eq. (11) with the value of u_+^f that gives $\lambda^f = 1$ in Eq. (9).

PARTICULAR SOLUTIONS FOR DST AND THEIR APPLICATION TO DDT

Particular solutions for DST are obtained from the previous equations by assigning values to the following set of parameters (ρ_o, c_o, q, v_o^p, m, α_m, A). The solutions presented here have the values $\rho_o = 1.6$ g/cc, $c_o = 2$ mm/μs, $q = 54.69$ kbar cc/g, $v_o^p = 8.4 \times 10^{-2}$ cc/g, $m = 1$, $\alpha = \alpha_1 = 2 \times 10^{-2}$ mm/μs^2, and values of the burning parameter A in the range 9.0×10^{-3} - 1.2×10^{-2} mm/μs kbar. The value q is based on an assumed Chapman-Jouguet pressure in the propellant of 350 kbar. Equations for the flow variables were evaluated for specified values of u_+^f. Equations (11) and (19) were used to calculate the flame path, Eqs. (4) through (7) and Eq. (20) were used to calculate states in the compression wave, Eqs. (19), (27), (28), (29),

and Eq. (9) were used to calculate values of the flow variables in the burnt state and the density behind the flame, and Eq. (31) was used to calculate values of the particle velocity behind the flame. The value of u_+^f was increased in these calculations until the reaction coordinate satisfied the condition $\lambda^f = 1$ to determine the reaction t_R and define the time limit imposed on the solution by the energy equation.

Plots of the particle velocity-distance profiles calculated with the following values of A, 1.2×10^{-2} mm/μs kbar, 1.1×10^{-2} mm/μs kbar, and 9.0×10^{-3} mm/μs kbar are shown in Figures 1, 2, and 3 to demonstrate the dependence of DST on this burning rate parameter. The flame path and the states connected by the flame with $A = 1.2 \times 10^{-2}$ mm/μs kbar are given in Table 1. For convenience in presentation, Figure 1 is shown on this page, but Figures 2 and 3 and the table are shown on the next page.

shown at 20 μs, 35 μs, and 52 μs. Because $\lambda^f = 1$ in the discontinuity shown as $F''_+F''_-$, the reaction time $t_R = 52$ μs for this flow. The particle velocity profiles FF'_- and FF''_- behind the flame are shown as straight lines to satisfy Eq. (30). Because $m = 1$, the shock is formed on the wave front at S where the particle velocity gradient becomes infinite after the time $t_s = 50$ μs given by Eq. (24). The flow therefore satisfies the condition $t_s < t_R$ because the shock is formed before the reaction goes to completion in the flame discontinuity. Our consideration of the shock after t_R, when the prescription of the flame acceleration is no longer valid, is based on the assumption that the flame can be treated as a constant velocity or decelerating piston. In either case, the information that the flame has undergone a change in its motion will be propagated along the C_+ characteristic emanating from the flame front when $t = t_R$. Points in the $(u_+ - x)$ profile F''_+C in Figure 1 will thus continue to propagate along C_+ character-

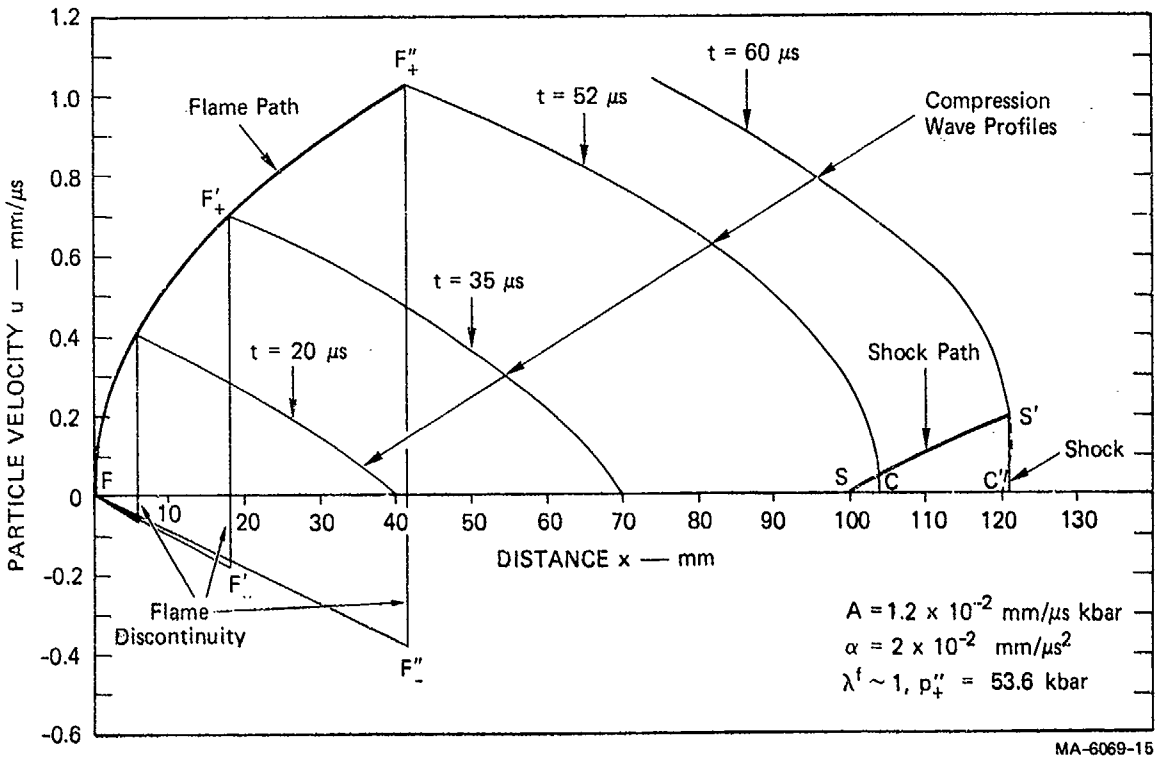

Figure 1. Flame path, shock path, and particle velocity-distance profiles for the flow produced by an accelerating flame with $A = 1.2 \times 10^{-2}$ mm/μs kbar.

The particle velocity-distance profiles shown in Figure 1 will now be considered in more detail to gain an insight into DST and formulate a postulate for assessing the probability of DDT. Figure 1 shows the formation and development of the shock produced by the accelerating flame when $A = 1.2 \times 10^{-2}$ mm/μs kbar. The flame path is shown as $FF'_+F''_+$ and the shock path as SS'. The positions of the flame discontinuity and the particle velocity profiles on both sides of the flame are

istics with velocities given by Eq. (7). The shock particle velocity and the position of the shock after a time $t > t_R = 50$ μs are defined by equalizing the areas in the double valued regions of the $(u_+ - x)$ profile as discussed earlier. The $(u_+ - x)$ profile S'C' at $t = 60$ μs in Figure 1 for example gives 0.2 mm/μs for the shock particle velocity and 121 mm for the position of the shock. The corresponding value of the shock pressure at $t = 60$ μs is 7.1 kbar. Application of this graphical method

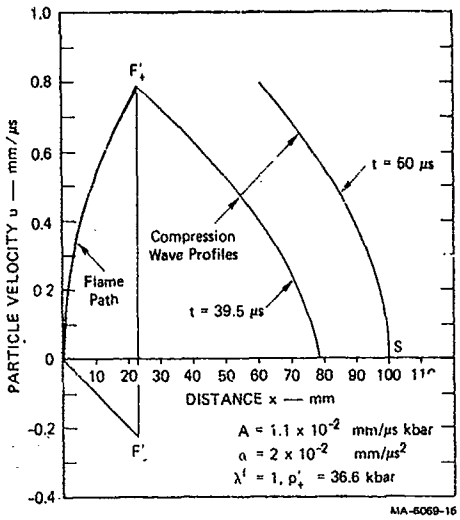

Figure 2: Particle velocity-distance profiles for the flow when the shock is formed and the reaction becomes complete in the accelerating flame with $A = 1.1 \times 10^{-2}$ mm/μs kbar.

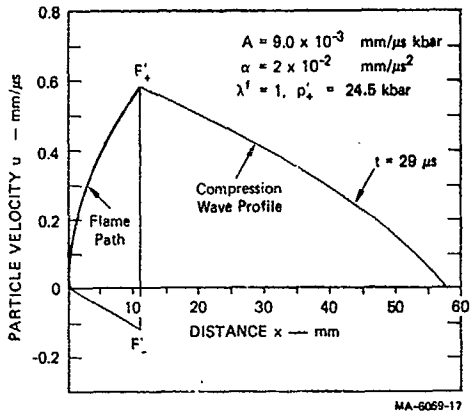

Figure 3: Particle velocity-distance profile for the flow when the reaction is complete in the accelerating flame with $A = 9.0 \times 10^{-3}$ mm/μs kbar.

u_+^f mm/μs	ρ_+^f/ρ_o	p_+^f kbar	x^i mm	t μsec
0.000E+00	1.000E+00	1.000E-03	0.000E+00	0.000E+00
1.000E-01	1.050E+00	3.364E+00	3.492E-01	5.000E+00
2.000E-01	1.100E+00	7.062E+00	1.410E+00	1.000E+01
3.000E-01	1.150E+00	1.111E+01	3.204E+00	1.500E+01
4.000E-01	1.200E+00	1.553E+01	5.751E+00	2.000E+01
5.000E-01	1.250E+00	2.033E+01	9.075E+00	2.500E+01
6.000E-01	1.300E+00	2.554E+01	1.320E+01	3.000E+01
7.000E-01	1.350E+00	3.116E+01	1.815E+01	3.500E+01
8.000E-01	1.400E+00	3.721E+01	2.395E+01	4.000E+01
9.000E-01	1.450E+00	4.371E+01	3.062E+01	4.500E+01
1.000E+00	1.500E+00	5.067E+01	3.820E+01	5.000E+01
1.040E+00	1.520E+00	5.359E+01	4.149E+01	5.200E+01

u_+^f mm/μs	ρ_-^f g/cc	p_-^f kbar	u_-^f mm/μs	λ^f
0.000E+00	4.439E-01	1.000E-03	-3.125E-05	4.436E-05
1.000E-01	4.699E-01	3.293E+00	-3.955E-03	1.409E-01
2.000E-01	4.967E-01	6.741E+00	-1.553E-02	2.781E-01
3.000E-01	5.245E-01	1.029E+01	-3.449E-02	4.095E-01
4.000E-01	5.531E-01	1.388E+01	-6.056E-02	5.529E-01
5.000E-01	5.827E-01	1.744E+01	-9.351E-02	6.463E-01
6.000E-01	6.132E-01	2.086E+01	-1.331E-01	7.476E-01
7.000E-01	6.445E-01	2.406E+01	-1.791E-01	8.349E-01
8.000E-01	6.768E-01	2.689E+01	-2.313E-01	9.063E-01
9.000E-01	7.099E-01	2.923E+01	-2.896E-01	9.599E-01
1.000E+00	7.439E-01	3.091E+01	-3.536E-01	9.938E-01
1.040E+00	7.577E-01	3.137E+01	-3.809E-01	1.002E+00

Table 1. Calculated values of the position of the flame and the states attained across the accelerating flame discontinuity with $A = 1.2 \times 10^{-2}$ mm/μs kbar.

to define the shock as the flow develops after t_R leads to the conclusion that the final shock pressure will be the pressure $p_+^u = 53.6$ kbar attained at the flame front when $t = t_R$. Consequently, in applying these solutions for an accelerating flame to DDT, we postulate that the pressure attained at the flame front when the reaction proceeds to completion in the flame can be used to assess the probability of the occurrence of DDT.

Particle velocity-distance profiles for flows when $A = 1.1 \times 10^{-2}$ mm/μs kbar and $A = 9.0 \times 10^{-3}$ mm/μs kbar are shown respectively in Figures 2 and 3. The flame trajectory and the particle velocity profile at t_R is shown in both figures, and it is clear from these profiles that $t_R < t_s$ for both these values of A. Figure 2 also shows the profile in the compression wave at 50 μs when the shock is formed. According to our postulate, the shock pressures for assessing the probability of DDT are respectively ~37 kbar and ~25 kbar when $A = 1.1 \times 10^{-2}$ mm/μs kbar and $A = 9.0 \times 10^{-3}$ mm/μs kbar.

The shock pressures for assessing the probability of DDT is our three flows are therefore 54 kbar, ~37 kbar, and ~25 kbar. While DDT is expected to occur when the shock pressure is 54 kbar or 37 kbar, it may not occur when the shock pressure is 25 kbar. The dependence of the pressure at the flame front on A when $t = t_R$ shows that the probability of the occurrence of DDT depends strongly on the burning rate, and leads to the conclusion that DDT will probably not occur in a closed tube when $A < 0.9 \times 10^{-3}$ mm/μs kbar.

RESULTS AND CONCLUSIONS

Solutions describing the one-dimensional unsteady flow produced by an accelerating flame propagating in a propellant or explosive contained in a closed tube were constructed to model DST and gain an insight into DDT. The flame was treated as a reactive discontinuity, the flow in front of the flame was treated as a simple compression wave, and the density gradient was assumed to be zero in the flow behind the flame. The description of the flow is phenomenological because the burning rate, the acceleration of the flame, and the density gradient behind the flame must be prescribed to construct the solution, but it supercedes thermodynamic treatments by accounting for the flow behind the flame as well as the flow in front of it. A graphical method was applied to the particle velocity profiles in the compression wave to determine the development of the shock ahead of the flame. Particular solutions were constructed over the time interval $0 \leq t \leq t_R$ defined by the time t_R taken for the reaction to proceed to completion in the flame discontinuity. It is not worthwhile to consider detailed properties of these solutions after the reaction time t_R because the equation used to prescribe the acceleration of the flame is not valid after this time. The postulate that the pressure attained at the flame front when $t = t_R$ can be used to assess the probability of DDT was based on the assumption that the flame can be treated as a constant velocity or decelerating piston after t_R. Examination of particular solutions in the light of this postulate led to the following conclusions:

- DDT depends strongly on the burning rate and will probably not occur unless the burning rate parameter exceeds a critical value.
- A burning rate governing by the square of the pressure is not necessary for the onset of DDT in a closed tube.

The model solutions constructed in this paper for the flow associated with an accelerating reactive flame discontinuity provide guidelines for assessing the probability of the occurrence of DDT in a burning propellant contained in a closed tube. Questions regarding the applicability of these solutions to real systems must be considered however because the extent of reaction in the flame discontinuity increases as the flow develops. It is my conjecture that the assumptions made to treat the flow may be valid in a damaged or cast burning composite propellant when the components have markedly different reaction rates.

A more fundamental theoretical study of the flow produced by an unsteady flame must be undertaken to obtain a basic understanding of DDT. Questions regarding the treatment of a flame as a reactive discontinuity and the application of a steady-state burning rate expression to an unsteady flame must be addressed in this study, and a more complete treatment of the flow must be incorporated into a model for predicting the acceleration of the flame.

ACKNOWLEDGMENT

The author thanks B. Y. Lew for programming routines to calculate the flame trajectory and the states connected by the flame discontinuity.

REFERENCES

1. H. Jones, Accelerated Flames and Detonation in Gases, Proc. Roy. Soc. A 248, No. 1254, 333, 1958.

2. G. K. Adams and D. C. Pack, "Some Observations on the Problem of Transition Between Deflagration and Detonation," Seventh Symposium (International) on Combustion, Butterworths, London 1959, p. 812.

3. A. Macek, "Transition from Deflagration to Detonation in Cast Explosive," J. Chem. Phys. 31, 162, 1959.

4. C. M. Tarver. T. C. Goodale, R. Shaw, and M. Cowperthwaite, "Deflagration-to-Detonation Transition Studies for Two Potential Isomine Cast Primary Explosives," Proceedings of the Sixth Symposium (International) on Detonation, ACR-221, p. 231, Office of Naval Research, 1976.

5. I. D. Landau and E. M. Lifsnitz, Fluid Mechanics (Pergamon Press, London, Paris, Frankfurt, 1959, Addison-Wesley Publishing Company, Inc., Reading, Massachusetts) p. 374.